plate, and cortical bone in the treated MPSVII mice. Voglar *et al.* reported on the therapeutic effect of ERT on skeletal deformities during the neonatal period [12]. In their study, recombinant β-glucuronidase enzyme was administered intravenously into MPSVII mice at weekly intervals from birth to 6 weeks of age. Slight elimination of vacuolated osteocytes and osteoblasts was shown in the treated mice 14 days after the last injection of ERT. However, both BMT and ERT have limitations for the treatment of human MPSVII. For BMT, a shortage of suitable donors makes it difficult to apply widely. ERT requires frequent injections of the purified enzymes, which is very expensive in general. For these reasons, another treatment strategy has to be developed to improve skeletal deformities in MPSVII.

Recently, gene therapy for MPSVII including *in vivo* and *ex vivo* gene transduction approaches has been attempted using several viral vectors such as retroviruses [13–19], herpesviruses [20,21], adenoviruses [22–29], lentiviruses [30,31], and adeno-associated viruses [32–35]. Several types of cells, such as bone marrow cells [16], fibroblasts [17], and myoblasts [18], were transduced with retroviral vectors, and the cells overexpressing GUSB were administered into adult MPSVII mice locally as well as systemically. Limited correction of lysosomal storage in the liver and spleen was demonstrated following these *ex vivo* gene therapies. An *in vivo* gene therapy approach has also been successful for generating tissues overexpressing GUSB. We administered an E1/E3-deleted adenoviral vector expressing GUSB (AxCAhGUS) into MPSVII mice via the tail vein and demonstrated that high levels of GUSB were observed in the liver, spleen, kidney, lung, and heart [27].

We previously reported that intravenous administration of AxCAhGUS during the neonatal period was sufficient to improve facial and cranial bone deformities in mice with MPSVII [29]. Ponder *et al.* described remarkable improvement of skeletal-articular lesions in dogs with MPSVII after retroviral gene transfer shortly after birth [19]. Daly *et al.* also reported that AAV-mediated gene transfer during the neonatal period resulted in a remarkable improvement of characteristic phenotypes, such as flattered face, hunched stature, and shortening of bone length [35]. However, the therapeutic effect on skeletal deformities and growth retardation, the major symptoms in MPSVII, was not fully investigated by biochemical and histopathological analysis in these papers.

Here, we administered AxCAhGUS intravenously and evaluated the therapeutic effects on skeletal deformities and growth retardation in mice with MPSVII. These analyses demonstrate that the improvement of growth disturbance and pathological correction of the articular cartilage and growth plate are achievable by a single adenoviral administration into neonatal MPSVII mice.

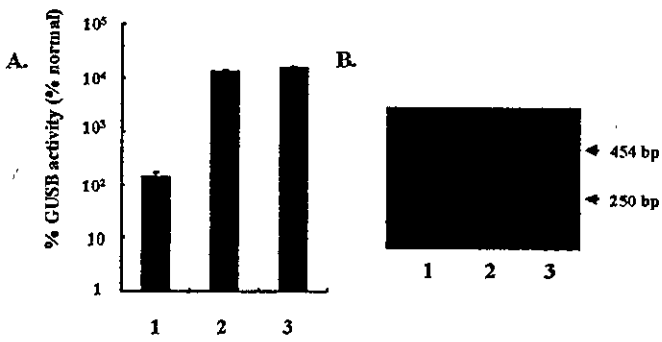

FIG. 1. Therapeutic efficacy in the articular cartilage of B6/MPSVII mice infected with AxCAhGUS in adulthood. (A) We injected 1.0 ml of viral solution containing 1×10^8 pfu of AxCAhGUS into adult B6/MPSVII mice (12–15 weeks of age). The mice were sacrificed 7 days after intravenous administration. The GUSB activities in the articular cartilage (lane 1), liver (lane 2), and serum (lane 3) were measured. Results are expressed as the percentage of GUSB activity found in the corresponding organs from four age-matched B6 (+/+) mice. (B) DNA from the articular cartilage and liver was extracted and used as templates for PCR. Virally encoded human GUSB cDNA in AxCAhGUS produced a 240-bp band, and the murine GUSB gene produced a 454-bp band. Both 454- and 240-bp DNA fragments were amplified when PCR was performed using DNA from the liver as templates, while a single 454-band was amplified by PCR using DNA from the articular cartilage as templates. In each group, four mice were used, and representative results are shown (lane 1, liver; lane 2, articular cartilage; lane 3, articular cartilage).

Results

Therapeutic Effect on Articular Cartilage of the MPSVII Mice Treated in Adulthood

To evaluate the therapeutic efficacy of adenovirus-mediated gene therapy on articular cartilage of MPSVII mice, we sacrificed the gene-transduced adult B6/MPSVII mice 7 days after intravenous administration of 1×10^8 plaque-forming units (pfu) of AxCAhGUS. We determined GUSB activity using 4-methylumbelliferyl β-D-glucuronide as substrate. We observed high levels of GUSB activity (1.5-fold higher than normal GUSB activity) in the articular cartilage (Fig. 1A, lane 1). In the liver, high levels of GUSB activity were also detected (Fig. 1A, lane 2). Moreover, to determine whether the origin of GUSB activity in the articular cartilage was due to transgene expression or due to cross-correction of lysosomal GUSB, we performed a PCR-based assay to detect virally encoded DNA in the articular cartilage. The PCR primers were designed based on the sequences of exon 6 and exon 7 of the human GUSB gene to amplify a 240-bp fragment from the human GUSB cDNA in the viral genome of AxCAhGUS. This PCR also generates a 454-bp fragment from the endogenous murine GUSB gene [27]. The 454-bp DNA fragment corresponding to the partial endogenous murine GUSB gene was amplified; however, the 240-bp partial human GUSB cDNA located in AxCAhGUS was not amplified (Fig. 1B) from the DNA of the articular cartilage, suggesting that GUSB detected in the articular cartilage was the result of

doi:10.1016/S1525-0016(03)00262-4

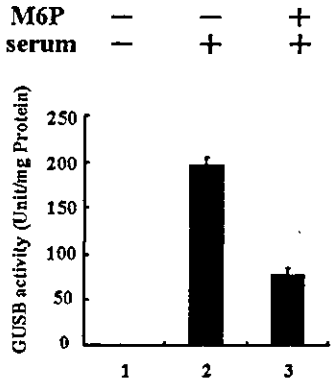

FIG. 2. Mannose 6-phosphate receptor-mediated endocytosis of GUSB in mouse chondrocytes. The articular cartilage from untreated MPSVII mice was incubated with medium with the serum from MPSVII mouse injected with 1×10^8 pfu of AxCAhGUS 7 days before. The serum contained 3.1×10^3 units of GUSB. The GUSB activity in the articular cartilage incubated with the serum was dramatically increased (lane 2); however, the increase was significantly suppressed when the articular cartilage was incubated in the presence of 6 mM mannose 6-phosphate (lane 3). The endogenous GUSB activity in the articular cartilage of MPSVII mice was negligible (lane 1).

in vivo cross-correction rather than direct gene transduction.

GUSB Cross-correction Mediated by the Mannose 6-phosphate Receptors in Chondrocytes

Cross-correction of many lysosomal enzymes is mediated mainly by the mannose 6-phosphate receptors expressed on cell surface membranes, and this process is efficiently blocked by mannose 6-phosphate [27]. To confirm that cross-correction mediated by mannose 6-phosphate receptors contributed to the high levels of GUSB activity in the articular cartilage of the treated MPSVII mice, we cocultured articular cartilage of the untreated MPSVII mice with medium containing serum obtained from the gene-transferred MPSVII mice. The GUSB activity was dramatically increased in the articular cartilage cocultured with serum containing 3.1×10^3 units of GUSB (Fig. 2, lane 2). Furthermore, the increase in GUSB activity was significantly reduced when 6 mM mannose 6-phosphate was present in the medium (Fig. 2, lane 3). These observations suggest that the GUSB enzyme was taken up by articular chondrocytes via the mannose 6-phosphate receptors.

Therapeutic Effects on Skeletal Deformities and Growth Retardation after Administration of AxCAhGUS during the Neonatal Period

Intravenous administration of AxCAhGUS in adulthood has little effect on growth retardation and skeletal deformities in MPSVII mice, because skeletal deformities and growth retardation are progressive from the neonatal period in mucopolysaccharidoses. To prevent skeletal deformities and growth retardation from progressing in MPSVII mice, we started treatment during the neonatal period. We injected 1×10^7 pfu of AxCAhGUS via the superficial temporal vein into the newborn MPSVII mice within 24 h of delivery and evaluated the therapeutic effect on skeletal deformities and growth retardation. Long-term observation (140 days after the treatment) demonstrated a remarkable improvement of growth retardation in the mice treated during the neonatal period (Fig. 3A2). The lengths of the tibia and fibula of the treated MPSVII mice were almost indistinguishable from those of their normal littermates (Fig. 3B2). These results demonstrate that morphological normalization of skeletal deformities in MPSVII is apparently achievable when the treatment starts during the neonatal period.

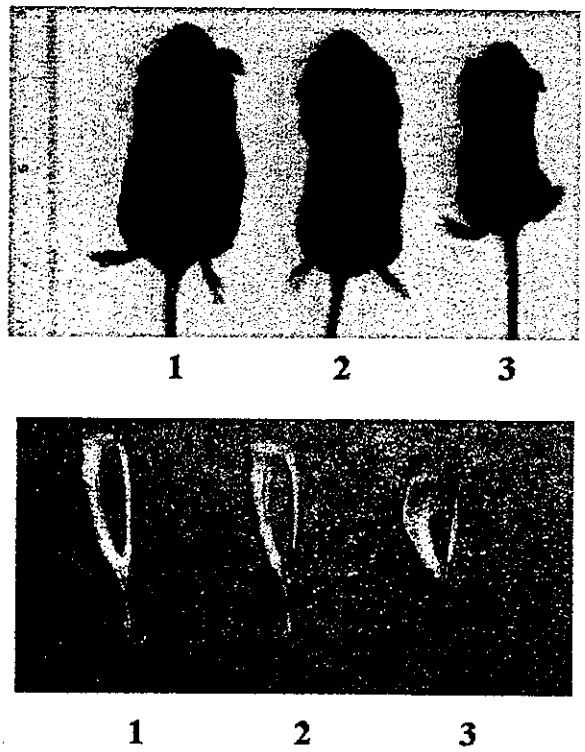

FIG. 3. Therapeutic effect on skeletal deformities and growth retardation in neonatally treated mice with MPSVII. (A) Growth retardation is a characteristic symptom of mice with B6/MPSVII. We injected 100 μl of viral solution containing 1×10^7 pfu of AxCAhGUS via the superficial temporal vein into neonatal B6/MPSVII mice within 24 h of delivery and evaluated the therapeutic effect on skeletal deformities and growth retardation 140 days after the treatment. The body length of the treated MPSVII mice (2) was indistinguishable from that of a B6 (+/+) littermate (1), while an untreated MPSVII littermate looked remarkably short (3). (B) The shape and length of the tibia and fibula of the neonatally treated mice (2) were compared with those of their affected (3) or normal (1) littermates. The long bones of the MPSVII mice (3) were significantly short and wide compared with those of their normal littermates (1), and the long bones of the treated MPSVII mice (2) show length and shape similar to those of their normal littermates.

Biochemical Analysis of Articular Cartilage in the Mice Treated during the Neonatal Period

To evaluate the therapeutic effect on skeletal deformities in more detail, we performed biochemical analysis. We sacrificed MPSVII mice treated during the neonatal period 30 days after the treatment and measured GUSB activities in the articular cartilage and liver (Figs. 4A and 4B). We observed high levels of GUSB activity (631.9 ± 69.9 unit/mg protein) corresponding to more than threefold higher than normal GUSB activity in the articular cartilage of the treated mice (Fig. 4A, lanes 1 and 2). In the liver, high levels of GUSB activity were also detected (Fig. 4A, lanes 3 and 4). We isolated chondrocytes from the articular cartilage of MPSVII mice and performed GUSB activity staining on the chondrocyte culture. About 40% of the chondrocytes from the MPSVII mice treated with AxCAhGUS were GUSB-positive cells (Fig. 4B). PCRs demonstrated that viral DNA was detectable in the articular cartilage of the MPSVII mice treated during the neonatal period (Fig. 4C). These results suggested that the articular cartilage was efficiently transduced with an adenoviral vector and extremely high levels of transgene expression could be obtained, when the mice were treated during the neonatal period.

Histopathological Analysis of Skeletal Lesions in the Mice Treated during the Neonatal Period

We compared histopathological analysis in the knee joint after the neonatal treatment (Figs. 5B, 5E, and 5H) with age-matched normal (Figs. 5A, 5D, and 5G) and untreated MPSVII mice (Figs. 5C, 5F, and 5I). Extensive vacuolization of the cells in the articular cartilage was not completely eliminated; however, they were obviously reduced in size and number after the treatment (Fig. 5B). The normal columnar architecture in the growth plate (resting zone, proliferative zone, hypertrophic zone, and endochondral; bone) was completely disrupted in the untreated MPSVII mice (Fig. 5F); however, we observed columnar architecture in the proliferative and hypertrophic zones in the MPSVII mice treated with neonatal gene therapy (Fig. 5E). Subchondral bone and bone marrow cells near the articular surface were significantly improved in the treated MPSVII mice (Fig. 5H). These results demonstrate that limited but significant improvement of pathological lesions in bone tissues was achieved in the gene-transduced MPSVII mice.

Discussion

Skeletal deformities and growth retardation are frequent manifestations of mucopolysaccharidoses. Multiple skeletal abnormalities, including short stature, angular deformities of the ribs, abnormally short forelimbs, subluxation of the hip joints, and epiphyseal dysplasia involving the vertebrae and long bones were observed in feline and murine models of MPSVII [4,36].

The pathogenesis of skeletal deformities and growth retardation was studied using several models of mucopolysaccharidoses [37,38]. Abreu *et al.* reported that clusters of distended chondrocytes disrupted the normal columnar architecture of the growth plate, presumably leading to bone growth abnormalities [37]. Simonaro *et al.* demonstrated that accumulated dermatan sulfate in the chondrocytes enhanced apoptosis of the articular cartilage cells in MPSVI cats, leading to degeneration of the articular surface [38]. These results suggest that abnormal chondrocytes in the articular cartilage and growth plate play an important role in skeletal deformities and growth retardation in mucopolysaccharidoses.

Recently, several reports have demonstrated that neonatal gene therapy contributed to a remarkable improvement of skeletal deformities in MPSVII mice [19,29,35]. However, histopathological and biochemical analyses of the skeletal lesions were not performed in these reports. Here, we demonstrated improvements in skeletal architecture and bone pathology in MPSVII mice by adenovirus-mediated gene therapy during the neonatal period.

Histopathological abnormality of the growth plate has been well characterized in other types of mucopolysaccharidoses [37,39]. Abreu *et al.* reported that poorly organized proliferative and hypertrophic zones were observed in the growth plate of MPSVI cats [37]. Silvery *et al.* also reported that the normal columnar architecture of the proliferative and hypertrophic zones was disrupted in the growth plate of a human patient with Hurler's syndrome [39]. In this study, almost total loss of the proliferative and hypertrophic zones was shown in the growth plate of untreated MPSVII mice, while a columnar architecture of the proliferative and hypertrophic zones was demonstrated in the growth plate of MPSVII mice following neonatal gene therapy. These results suggest that pathological improvement of the proliferating and hypertrophic zones in the growth plate is important for the normalization of growth retardation and bone development in MPSVII mice treated by neonatal gene transfer.

Moreover, biochemical analysis of the articular cartilage was performed following adult and neonatal gene therapy. When we injected adenoviral vectors into adult MPSVII mice, most of the vectors were distributed predominantly in the liver [27]. The GUSB enzyme was secreted mainly from hepatic cells and significantly taken up by other cells via the mannose 6-phosphate receptors expressed on the cell surface membrane. This pathway is called *in vivo* cross-correction. Our results demonstrated that this *in vivo* cross-correction mechanism also contributed to high levels of GUSB activity in the articular cartilage of the treated MPSVII mice following adult gene therapy. On the other hand, we previously reported that adenoviral vectors were distributed in multiple organs such as the liver, lung, heart, spleen, kidney, and brain in MPSVII mice treated by neonatal gene therapy [29]. In this study, a PCR-based method demonstrated that viral

doi:10.1016/S1525-0016(03)00262-4

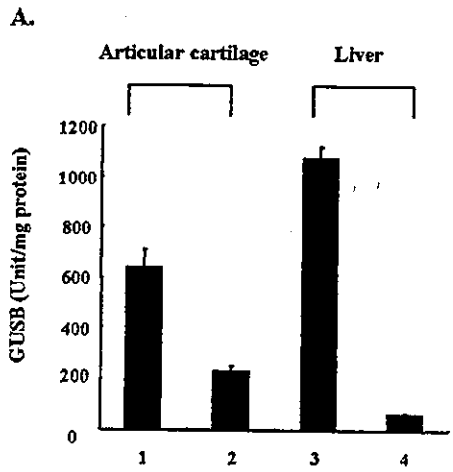

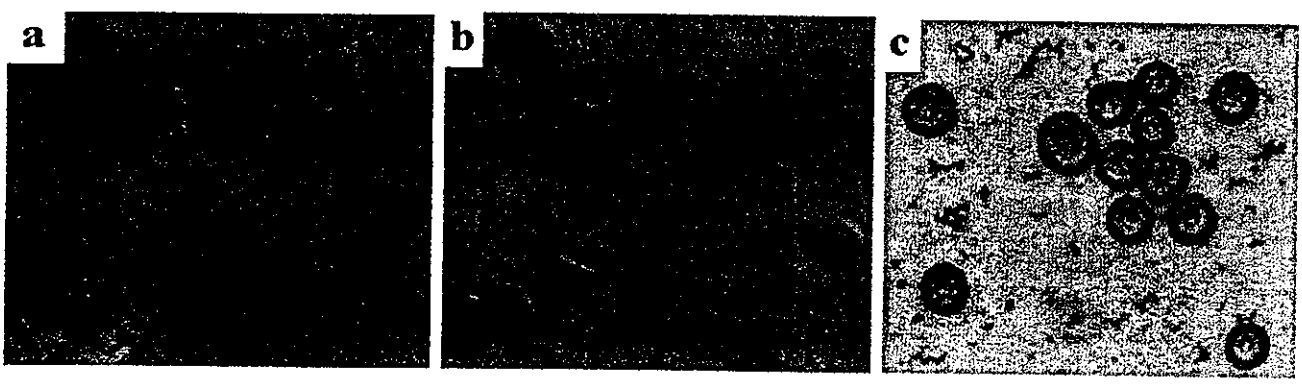

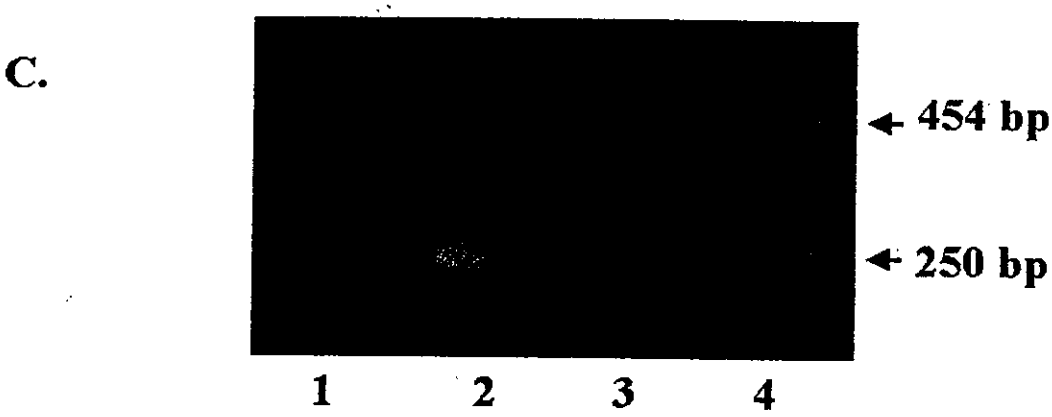

FIG. 4. Biochemical analysis of the articular cartilage of B6/MPSVII mice infected with AxCAhGUS in the neonatal period. (A) The mice treated during the neonatal period were sacrificed 30 days after the treatment and the GUSB activity in the articular cartilage and liver was measured. High levels of GUSB activity were observed in the articular cartilage (lane 1) and liver (lane 3) of the treated mice. (Lane 1, articular cartilage from the treated mice; lane 2, articular cartilage from normal B6 mice; lane 3, liver from the treated mice; lane 4, liver from normal B6 mice.) (B) Biochemical analysis with naphthol AS-BI β-*d*-glucuronide was also performed. Only GUSB-positive cells were observed in cells of B6 (+/+) mice (a). GUSB-positive chondrocytes (stained red) were identified in the treated MPSVII mice (b), while no GUSB-positive cells were observed in untreated MPSVII mice (c). (C) DNA from chondrocytes and livers was extracted and used as templates for PCR. Virally encoded human GUSB cDNA in AxCAhGUS generated a 240-bp band, and the murine GUSB gene produced a 454-bp band. Both the 240- and the 454-bp DNA fragments were amplified in both the articular cartilage and the liver. In each group, two mice were used for this experiment, and representative results are shown (lanes 1 and 2, liver; lane 3, articular cartilage; lane 4, articular cartilage).

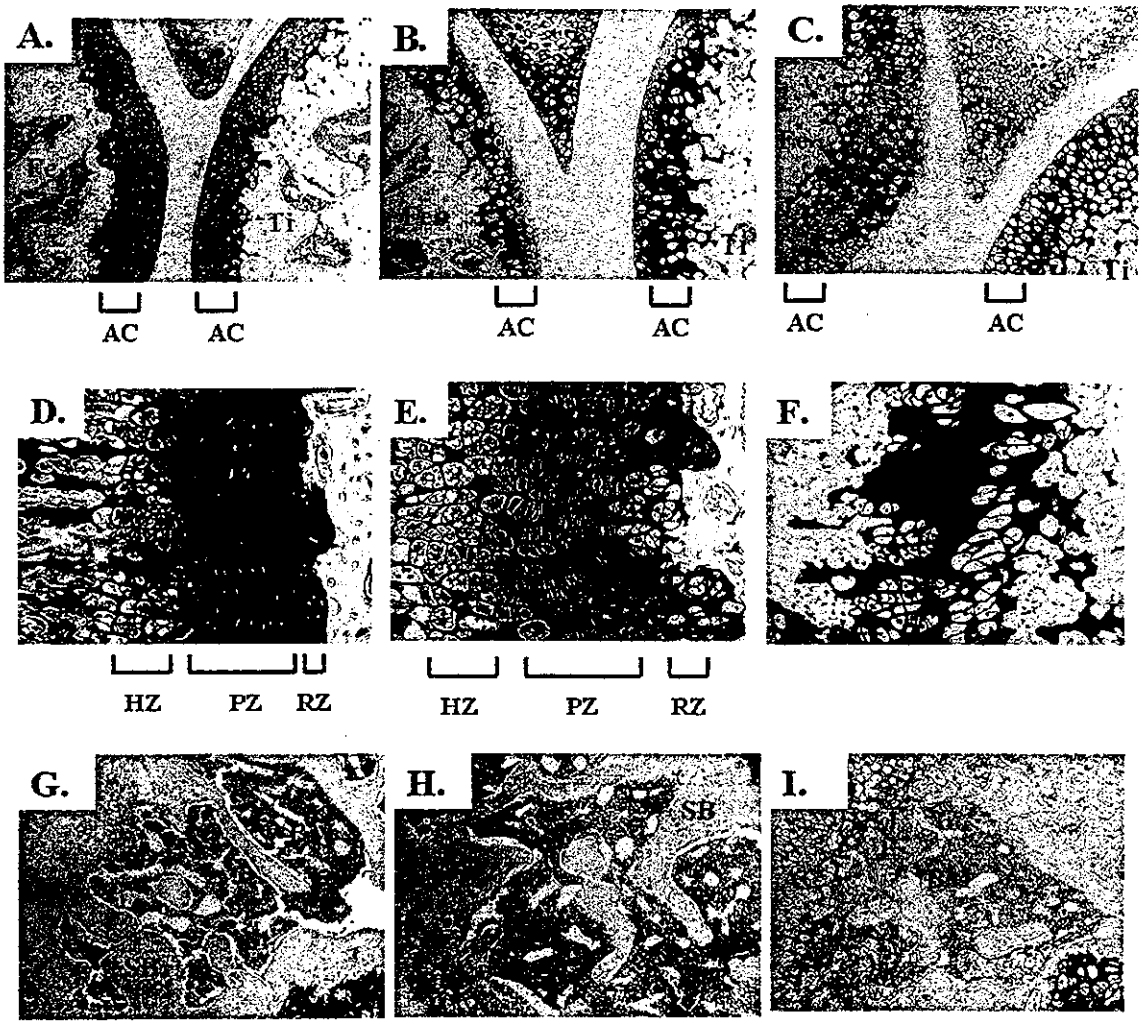

FIG. 5. Histopathological analysis of the epiphysis and metaphysis of the knee joint of B6/MPSVII mice treated with AxCAhGUS during the neonatal period. The mice that received adenoviral vectors during the neonatal period were sacrificed 30 days after the treatment, and pathological improvement in the articular cartilage and growth plate of the knee joint was evaluated. Toluidine blue staining of the epiphysis of normal mice (A), MPSVII mice 30 days after the treatment (B), and untreated MPSVII mice (C) is shown. Original magnification ×10. Moderate elimination of vacuole cells in the articular cartilage was observed in the treated mice with MPSVII. Toluidine blue staining of the metaphysis of normal mice (D), MPSVII mice 30 days after the treatment (E), and untreated MPSVII mice (F) is shown. Original magnification ×20. Moderate elimination of vacuole cells in the growth plate was also observed in the treated mice with MPSVII. Hematoxylin–eosin staining of the subchondral bone of normal mice (G), MPSVII mice 30 days after the treatment (H), and untreated MPSVII mice (I) is shown. Original magnification ×20. The subchondral bone near the articular surface was almost normal in the treated MPSVII mice. AC, articular cartilage; Fe, femur; Ti, tibia; GP, growth plate; RZ, resting zone; PZ, proliferative zone; HZ, hypertrophic zone; SB, subchondral bone; BM, bone marrow.

DNA was also detected in the articular cartilage after neonatal gene transfer. This result means that high levels of GUSB activity detected in the articular cartilage are not only due to *in vivo* cross-correction, but also due to transgene expression following neonatal gene therapy.

Successful *in vivo* gene transduction into murine articular chondrocytes during the neonatal period is the most important finding in this study. Gene transduction into the articular tissues has been already reported [40–42]. Arai *et al.* demonstrated *ex vivo* gene transduction into murine articular chondrocytes using adenoviral vectors [40]. In their study, efficient transgene expression was observed in the chondrocytes for at least 21 days. However, *in vivo* gene transduction into the articular chondrocytes was not successful when an intra-articular injection of viral vectors was carried out in adulthood [41,42].

There is a significant difference in the characterization of articular cartilage between adult and neonatal mice. The articular cartilage consists of sparse chondrocytes and a dense extracellular matrix. Each chondrocyte in the articular cartilage is isolated to its own lacuna and is surrounded by the extracellular matrix. The articular car-

doi:10.1016/S1525-0016(03)00262-4

tilage in adulthood is an avascular area and is nourished by synovial fluid diffusion. However, the articular cartilage during the neonatal period is adequately supplied with epiphyseal vessels [43]. When an intravenous administration of AxCAhGUS was given to neonatal MPSVII mice, the vector could transduce the articular chondrocytes via the artery.

To prevent the progression of skeletal deformity and growth retardation in MPSVII mice, persistent high levels of GUSB activity in the skeletal lesion should be maintained for at least 4 weeks after neonatal treatment, because the growth period of these mice is usually from birth to 4–8 weeks of age. In this paper, high levels of GUSB activity were observed in the articular cartilage 30 days after neonatal gene transfer. Moreover, we previously demonstrated the time-dependent change of serum GUSB activity in mice infected with AxCAhGUS during the neonatal period [29]. In that report, high levels of GUSB activity (10-fold higher than normal GUSB activity) were also observed in sera from treated mice 5 weeks after neonatal administration of AxCAhGUS. These results suggest that the persistent high levels of GUSB activity in MPSVII mice during the neonatal period are sufficient for not only histopathological improvement of articular cartilage and growth plate, but also remarkable improvement of growth retardation in MPSVII mice following neonatal gene therapy.

Here, we demonstrated the therapeutic effect on skeletal abnormalities using a murine model of MPSVII. It is important to prevent skeletal deformities from progressing in mucopolysaccharidoses and neonatal treatment is desirable for this purpose. Although several safety issues have to be resolved before clinical application, this neonatal gene therapy using an adenoviral vector is a promising strategy for treating the skeletal deformities of MPS-VII and other lysosomal storage diseases.

Materials and Methods

Generation of a recombinant adenovirus expressing human GUSB. An adenovirus, AxCAhGUS, for human GUSB was constructed by the COS-TPC method described previously [27]. A cosmid, AxCAhGUS, which contained an expression cassette of human GUSB under the control of the CAG promoter, was constructed by subcloning cDNA for human GUSB at a unique *SwaI* site of pAxCAwt. 293 cells were cotransfected with cosmid pAxCAhGUS and the adenovirus DNA-terminal protein complex, which had already been digested at several sites with *Eco*T22I. A recombinant adenovirus was generated through homologous recombination in the 293 cells.

Animals. Syngeneic B6 (+/+) and B6/MPSVII (mps/mps) mice were obtained from a pedigree colony of B6.C-H-2^{bm1}/ByBir-gus^{mps}/+ maintained at the National Research Institute of Child Health and Development. All mice were maintained in accordance with the guidelines of the animal committee of the facility.

Quantitative analysis of GUSB in the articular cartilage and liver. The articular cartilage was removed from the bilateral patella, femoral head, and humeral head. The articular cartilage and liver were washed in Dulbecco's modified Eagle's medium (DMEM; Nissui Pharmaceutical, Tokyo, Japan). GUSB activities were measured in tissue homogenates using a fluorometric assay described previously [44]. Briefly, pellets were homogenized in 10 mM Tris–HCl (pH 7.5), 150 mM NaCl, 0.2% Triton X-100, and 1 mM dithiothreitol and centrifuged at 14,000 rpm for 1min to remove debris. The GUSB activities were measured using 4-methylumbelliferyl β-*d*-glucuronide (Sigma, St. Louis, MO) as substrate.

Isolation of chondrocytes from the articular cartilage and GUSB activity staining of the articular chondrocytes. Chondrocytes were isolated as previously described [40]. The articular cartilage was cut into pieces in DMEM supplemented with 10% fetal bone serum (FBS; Gibco BRL, Gaithersburg, MD), and treated with 0.025% collagenase and incubated at 37°C until the fragment was digested. Residual multicellular aggregates were removed by centrifugation, and cells were washed three times in DMEM, 5% FBS before the experiments. The chondrocytes were incubated in 24-well plates with a total volume of 1 ml of DMEM supplemented with 10% FBS for 2 days. GUSB activity staining was performed on the chondrocyte culture using naphthol AS-BI β-*d*-glucuronide (Sigma) as substrate, as previously described [27].

Detection of viral DNA in the articular cartilage. Total DNA of the tissue samples was extracted using a QIAamp DNA mini kit (Qiagen GmbH, Hilden, Germany) according to the manufacturer's protocol. Viral DNA of AxCAhGUS was detected using PCR to amplify the partial cDNA for human GUSB. The forward and reverse primers were synthesized based on the sequences of exon 6 (5′-CTGTGGCTGTCACCAAGAGC-3′) and exon 7 (5′-GGACACTCATCGATGACCAC-3′) of human GUSB cDNA. The sequences were identical to those of human cDNA, but had two mismatches within the murine exon 6 sequence. One hundred microliters of the PCR mixture contained 250 μM dNTPs, 10 pmol of the forward and reverse primers, 1 μg of purified DNA, and 2.5 U of *Taq* DNA polymerase (TaKaRa). Thirty cycles of PCR were carried out at 94°C for 90 s, 56°C for 90 s, and 72°C for 90 s. The expected products were a 240-bp fragment from cDNA and a 454-bp fragment from the endogenous murine gene.

Histopathology of the knee joints. Mice were sacrificed by cervical dislocation. Thereafter, the knee joints were removed and fixed in 10% formalin. After decalcification in 5% formic acid, the specimens were embedded in paraffin, sectioned at 5 μm, and stained with toluidine blue and hematoxylin–eosin. Histopathological sections were evaluated morphologically by light microscopy [40].

Acknowledgments

We thank Drs. Y. Kanegae and I. Saito for recombinant adenovirus constructs and Dr. J. Miyazaki for the CAG promoters. This work was supported in part by grants for Pediatric Research from the Ministry of Health, Labor, and Welfare, Japan, and by grants for Research on Health Sciences Focusing on Drug Innovation from the Japan Health Sciences Foundation.

RECEIVED FOR PUBLICATION MAY 27, 2003; ACCEPTED JULY 28, 2003.

References

1. Sly, W. S., Quinton, B. A., McAlister, W. H., and Rimoin, D. L. (1973). β-Glucuronidase deficiency: report of clinical, radiologic, and biochemical features of a new mucopolysaccharidosis. *J. Pediatr.* **82**: 249–257.
2. Birkenmeier, E. H., *et al.* (1989). Murine mucopolysaccharidosis type VII: characterization of a mouse with beta-glucuronidase deficiency. *J. Clin. Invest.* **83**: 1258–1266.
3. Sands, M. S., and Birkenmeier, E. H. (1993). A single-base-pair deletion in the beta-glucuronidase gene accounts for the phenotype of murine mucopolysaccharidosis type VII: a single-base-pair deletion in the beta-glucuronidase gene accounts for the phenotype of murine mucopolysaccharidosis type VII. *Proc. Natl. Acad. Sci. USA* **90**: 6567–6571.
4. Vogler, C., *et al.* (1990). A murine model of mucopolysaccharidosis VII: gross and microscopic findings in beta-glucuronidase-deficient mice. *Am. J. Pathol.* **136**: 207–217.
5. Sands, M. S., *et al.* (1997). Gene therapy for murine mucopolysaccharidosis type VII. *Neuromuscul. Disord.* **7**: 352–360.
6. Birkenmeier, E. H., *et al.* (1991). Increased life span and correction of metabolic defects in murine mucopolysaccharidosis type VII after syngeneic bone marrow transplantation. *Blood* **78**: 3081–3092.
7. Sands, M. S., *et al.* (1994). Enzyme replacement therapy for murine mucopolysaccharidosis type VII. *J. Clin. Invest.* **93**: 2324–2331.

8. Vogler, C., *et al.* (1997). Murine mucopolysaccharidosis type VII: long term therapeutic effects of enzyme replacement and enzyme replacement followed by bone marrow transplantation. *J. Clin. Invest.* **99**: 1596–1605.
9. Vogler, C., *et al.* (1999). Enzyme replacement in murine mucopolysaccharidosis type VII: neuronal and glial response to β-glucuronidase requires early initiation of enzyme replacement therapy. *Pediatr. Res.* **45**: 838–844.
10. O'Conner, L. H., *et al.* (1998). Enzyme replacement therapy for murine mucopolysaccharidosis type VII leads to improvement in behavior and auditory function. *J. Clin. Invest.* **101**: 1394–1400.
11. Sands, M. S., *et al.* (1993). Treatment of murine mucopolysaccharidosis type VII by syngeneic bone marrow transplantation in neonates. *Lab. Invest.* **68**: 676–686.
12. Vogler, C., Sands, M. S., Levy, B., Galvin, N. J., Birkenmeier, E. H., and Sly, W. S. (1999). Enzyme replacement with recombinant β-glucuronidase in murine mucopolysaccharidosis type VII: impact of therapy during the first six weeks of life on subsequent lysosomal storage, growth, and survival. *Pediatr. Res.* **45**: 838–844.
13. Gao, C., Sands, M. S., Harkins, M. E., and Ponder, K. P. (2000). Delivery of a retroviral vector expressing human β-glucuronidase to liver and spleen decreases lysosomal storage in mucopolysaccharidosis type VII mice. *Mol. Ther.* **2**: 233–244 , doi:10.1006/mthe.2000.0121..
14. Taylor, R. M., and Wolfe, J. H. (1997). Decreased lysosomal storage in the adult MPS VII mouse brain in the vicinity of grafts of retroviral vector-corrected fibroblasts secreting high levels of β-glucuronidase. *Nat. Med.* **3**: 771–774.
15. Taylor, R. M., and Wolfe, J. H. (1994). Cross-correction of β-glucuronidase deficiency by retroviral vector-mediated gene transfer. *Exp. Cell Res.* **214**: 606–613.
16. Marechal, V., Naffakh, N., Danos, O., and Heard, J. M. (1993). Disappearance of lysosomal storage in spleen and liver of mucopolysaccharidosis VII mice after transplantation of genetically modified bone marrow cells. *Blood* **84**: 1358–1365.
17. Moullier, P., Bohl, D., Heard, J. M., and Danos, O. (1993). Correction of lysosomal storage in the liver and spleen of MPSVII mice by implantation of genetically modified skin fibroblasts. *Nat. Genet.* **4**: 154–159.
18. Naffakh, N., Pinset, C., Montarras, D., Li, Z., Paulin, D., and Danos, O. (1996). Long-term secretion of therapeutic proteins from genetically modified skeletal muscles. *Hum. Gene Ther.* **7**: 11–21.
19. Ponder, K. P., *et al.* (2002). Therapeutic neonatal hepatic gene therapy in mucopolysaccharidosis VII dogs. *Proc. Natl. Acad. Sci. USA* **99**: 13102–13107.
20. Zhu, J., Kang, W., Wolfe, J. H., and Fraser, N. W. (2000). Significantly increased expression of beta-glucuronidase in the central nervous system of mucopolysaccharidosis type VII mice from the latency-associated transcript promoter in a nonpathogenic herpes simplex virus type 1 vector. *Mol. Ther.* **2**: 82–94, doi:10.1006/mthe.2000.0093.
21. Wolfe, J. H., Deshmane, S. L., and Fraser, N. W. (1992). Herpesvirus vector gene transfer and expression of β-glucuronidase in the central nervous system of MPS VII mice. *Nat. Genet.* **1**: 379–384.
22. Ghodsi, A., Stein, C., Derksen, T., Martins, I., Anderson, R. D., and Davidson, B. L. (1999). Systemic hyperosmolality improves β-glucuronidase distribution and pathology in murine MPS VII brain following intraventricular gene transfer. *Exp. Neurol.* **160**: 109–116.
23. Ghodsi, A., Stein, C., Derksen, T., Yang, G., Anderson, R. D., and Davidson, B. L. (1998). Extensive β-glucuronidase activity in murine central nervous system after adenovirus-mediated gene transfer to brain. *Hum. Gene Ther.* **9**: 2331–2340.
24. Ohashi, T., Watabe, K., Uehara, K., Sly, W. S., Vogler, C., and Eto, Y. (1997). Adenovirus-mediated gene transfer and expression of human beta-glucuronidase gene in the liver, spleen, and central nervous system in mucopolysaccharidosis type VII mice. *Proc. Natl. Acad. Sci. USA* **94**: 1287–1292.
25. Kosuga, M., *et al.* (2001). Engraftment of genetically engineered amniotic epithelial cells corrects lysosomal storage in multiple areas of the brain in mucopolysaccharidosis type VII mice. *Mol. Ther.* **3**: 139–148 , doi:10.1006/mthe.2000.0234..
26. Kosuga, M., *et al.* (2000). Phenotype correction in murine mucopolysaccharidosis type VII by transplantation of human amniotic epithelial cells after adenovirus-mediated gene transfer. *Cell Transplant.* **9**: 687–692.
27. Kosuga, M., *et al.* (2000). Adenovirus-mediated gene therapy for mucopolysaccharidosis VII: involvement of cross-correction in widespread distribution of the gene products and long-term effects of CTLA-4Ig coexpression. *Mol. Ther.* **1**: 406–413 , doi:10.1006/mthe.2000.0067..
28. Kamata, Y., *et al.* (2001). Adenovirus-mediated gene therapy for corneal clouding in mice with mucopolysaccharidosis type VII. *Mol. Ther.* **4**: 307–312 , doi:10.1006/mthe.2001.0461..
29. Kamata, Y., *et al.* (2003). Long-term normalization in the central nervous system, ocular manifestations, and skeletal deformities caused by a single systemic adenovirus injection into neonatal mice with mucopolysaccharidosis VII. *Gene Ther.* **10**: 406–414.
30. Stein, C. S., *et al.* (2001). In vivo treatment of hemophilia A and mucopolysaccharidosis type VII using nonprimate lentiviral vectors. *Mol. Ther.* **3**: 850–856 , doi:10.1006/mthe.2001.0325..
31. Bosch, A., Perret, E., Desmaris, N., Trono, D., and Heard, J. M. (2000). Reversal of pathology in the entire brain of mucopolysaccharidosis type VII mice after lentivirus-mediated gene transfer. *Hum. Gene Ther.* **11**: 1139–1150.
32. Sferra, T. J., *et al.* (2000). Recombinant adeno-associated virus-mediated correction of lysosomal storage within the central nervous system of the adult mucopolysaccharidosis type VII mouse. *Gene Ther.* **11**: 507–519.
33. Daly, T. M., Okuyama, T., Vogler, C., Haskins, M. E., Muzyczka, N., and Sands, M. S. (1999). Neonatal intramuscular injection with recombinant adeno-associated virus results in prolonged β-glucuronidase expression in situ and correction of liver pathology in mucopolysaccharidosis type VII mice. *Hum. Gene Ther.* **10**: 85–94.
34. Daly, T. M., Vogler, C., Levy, B., Haskins, M. E., and Sands, M. S. (1999). Neonatal gene transfer leads to widespread correction of pathology in a murine model of lysosomal storage disease. *Proc. Natl. Acad. Sci. USA* **96**: 2296–2300.
35. Daly, T. M., Ohlemiler, K. K., Roberts, M. S., Vogler, C., and Sands, M. S. (2001). Prevention of systemic clinical disease in MPSVII mice following AAV-mediated neonatal gene transfer. *Gene Ther.* **8**: 1292–1298.
36. Schultheiss, P. C., Gardner, S. A., Owens, J. M., Wenger, D. A., and Thrall, M. A. (2000). Mucopolysaccharidosis VII in a cat. *Vet. Pathol.* **37**: 502–505.
37. Abreu, S., *et al.* (1995). Growth plate pathology in feline mucopolysaccharidosis VI. *Calcif. Tissue Int.* **57**: 185–190.
38. Simonaro, C. M., Haskins, M. E., and Schuchman, E. H. (2001). Articular chondrocytes from animals with a dermatan sulfate storage disease undergo a high rate of apoptosis and release nitric oxide and inflammatory cytokines: a possible mechanism underlying degenerative joint disease in the mucopolysaccharidoses. *Lab. Invest.* **81**: 1319–1328.
39. Silveri, P., Kaplan, S., Fallon, D., Bayever, E., and August, S. (1991). Hurler syndrome with special reference to histologic abnormalities of the growth plate. *Clin. Orthop.* **269**: 305–311.
40. Arai, Y., *et al.* (1997). Adenovirus vector-mediated gene transduction to chondrocyte: in vitro evaluation of therapeutic efficacy of transforming growth factor-β1 and heat shock protein 70 gene transduction. *J. Rheumatol.* **24**: 1787–1795.
41. Watanabe, S., Imagawa, T., Boivin, G. P., Gao, G., Wilson, J., and Hirsch, R. (2000). Adeno-associated virus vector mediates gene transfer and delivery of chondroprotective IL-4 to murine synovium. *Mol. Ther.* **2**: 147–152 , doi:10.1006/mthe.2000.0111..
42. Gouze, E., *et al.* (2002). In vivo gene delivery to synovium by lentiviral vectors. *Mol. Ther.* **5**: 397–404.
43. Schiller, A. L. (1995). Pathology of Osteoarthritis: Osteoarthritic Disorder (In *K. E. Kunettner, and V. M. Goldgerg, Eds.), pp. 95–101. AAOS, Rosemont.*
44. Wolfe, J. H., and Sands, M. S. (1996). Murine mucopolysaccharidosis type VII: a model system for somatic gene therapy of the central nervous system. *Gene Transfer into Nervous System toward Gene Therapy of Neurological Disorders* (In *P. Lowenstain, and L. Enquist, Eds.), pp.263–274. Wiley, Essex, UK.*

nature
cell biology

MKK7 couples stress signalling to G2/M cell-cycle progression and cellular senescence

Teiji Wada[1,2], Nicholas Joza[1,2], Hai-ying M. Cheng[2], Takehiko Sasaki[2], Ivona Kozieradzki[2], Kurt Bachmaier[2], Toshiaki Katada[3], Martin Schreiber[4], Erwin F.Wagner[5], Hiroshi Nishina[3] and Josef M. Penninger[1,2,6]

During the development of multicellular organisms, concerted actions of molecular signalling networks determine whether cells undergo proliferation, differentiation, death or ageing. Here we show that genetic inactivation of the stress signalling kinase, MKK7, a direct activator of JNKs in mice, results in embryonic lethality and impaired proliferation of hepatocytes. Beginning at passage 4–5, *mkk7*$^{-/-}$ mouse embryonic fibroblasts (MEFs) display impaired proliferation, premature senescence and G2/M cell cycle arrest. Similarly, loss of c-Jun or expression of a c-JunAA mutant in which the JNK phosphorylation sites were replaced with alanine results in a G2/M cell-cycle block. The G2/M cell-cycle kinase CDC2 was identified as a target for the MKK7–JNK–c-Jun pathway. These data show that the MKK7–JNK–c-Jun signalling pathway couples developmental and environmental cues to CDC2 expression, G2/M cell cycle progression and cellular senescence in fibroblasts.

Mitogen-activated protein kinases (MAPKs) are a family of serine/threonine kinases that transduce signals from the cell membrane to the nucleus in response to a wide range of stimuli[1–7]. Two independent stress kinase signalling pathways — p38-MAPK and JNKs (c-Jun *N*-terminal kinase or SAPKs, stress-activated protein kinases) — participate in many different intracellular signalling pathways that control a spectrum of cellular processes, including cell growth, differentiation, transformation and apoptosis[1–7]. Both JNK-activation kinases — MKK4 and MKK7 — are required for full activation of JNK[8–10], and genetic inactivation of *mkk4* results in embryonic lethality with a liver defect between embryonic day 10.5 (E10.5) and E12.5 (ref. 11). However, nothing is known about the role of MKK7 in embryogenesis[12].

Here we show that genetic inactivation of MKK7 in mice results in defective hepatocyte proliferation and embryonic lethality. Inactivation of MKK7 in embryonic fibroblasts results in impaired proliferation, a G2/M cell-cycle arrest and premature senescence. The G2/M cell-cycle kinase CDC2 was identified as a molecular target for MKK7–JNK signalling. Loss of c-Jun or a expression of c-JunAA mutant in which the JNK phosphorylation sites were inactivates[13,14] also resulted in defective G2/M cell cycle progression and impaired CDC2 expression.

Table 1 Embronic lethality in *mkk7*$^{-/-}$ mice

	Litters	*mkk7*$^{+/+}$	*mkk7*$^{+/-}$	*mkk7*$^{-/-}$	Dead (%)	Total
E9.5	2	4	11	2	0 (0)	17
E10.5	2	5	8	5	0 (0)	18
E11.5	26	55	106	47	15 (31.1)	208
E12.5	**16**	**31**	**67**	**33**	**30 (90.9)**	131
E13.5	5	11	17	12	12 (100)	40
E16.5	1	3	4	0	–	7
1W	5	9	21	0	–	39

Embryos were isolated at the indicated time of gestation, analysed for viability and processed for histological staining. Genotypes of embryos were determined by PCR. Viability of embryos was determined by observing heart beating. E = embryonic day; 1W = 1 week after birth.

[1]IMBA (Institute of Molecular Biotechnology of the Austrian Academy of Sciences), c/o Dr. Bohrgasse 3-5, A-1030 Vienna, Austria. [2]University Health Network, Departments of Medical Biophysics and Immunology, University of Toronto, 620 University Avenue, Ontario M5G 2C1, Toronto, Canada. [3]Department of Physiological Chemistry, Graduate School of Pharmaceutical Sciences, University of Tokyo, 7-3-1 Hongo, Bunkyo-ku, 113-0033 Tokyo, Japan. [4]University of Vienna School of Medicine, Dept of Obstetrics and Gynecology Waehringer Guertel 18-20, A-1090 Vienna, Austria. [5]IMP (Research Institute of Molecular Pathology), Dr. Bohrgasse 7, A-1030 Vienna, Austria.
[6]Correspondence should be addressed to J.P. (e-mail: josef.penninger@oeaw.ac.at)

Published online: 22 February 2004; DOI: 10.1038/ncb1098

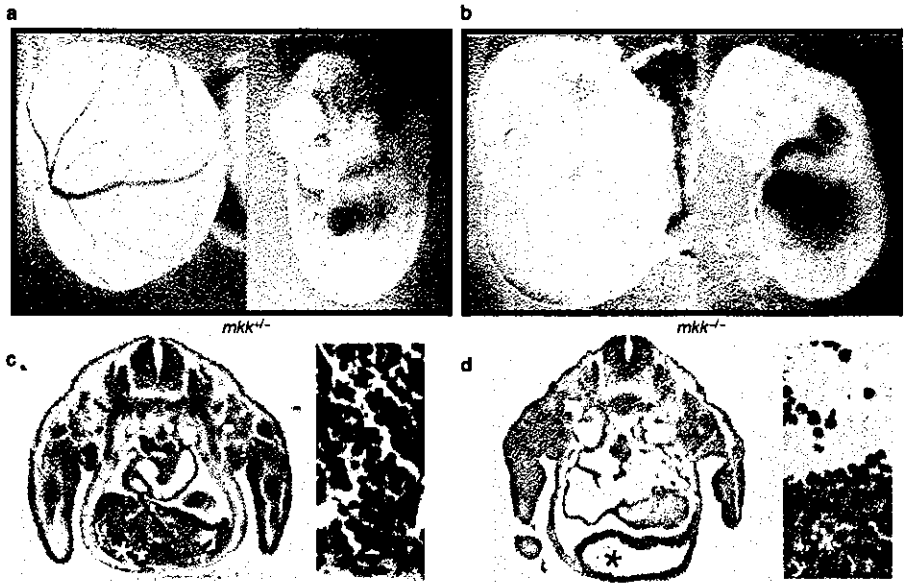

Figure 1 Impaired liver development in *mkk7*$^{-/-}$ embryos. (**a**, **b**) Macroscopic analysis of E11.5 *mkk7*$^{+/-}$ (**a**) and E11.5 *mkk7*$^{-/-}$ (**b**) littermate embryos. (**c**, **d**) Transverse sections of E11.5 *mkk7*$^{+/-}$ (**c**) and E11.5 *mkk7*$^{-/-}$ (**d**) embryos stained with H&E. Note the severe anaemia (**b**) and reduction of parenchymal hepatocytes in E11.5 *mkk7*$^{-/-}$ embryonic livers (asterisk in **c** and **d**). It should be noted that the liver structure and liver parenchyma are overtly normal in E9.5. Right panels show embryonic livers at higher magnifications (×100).

Table 2 Increased G2/M boundaries in *junAA* and *c-jun*$^{-/-}$ MEFs

Passages	2			4			6			
	mkk7$^{+/-}$	*mkk7*$^{-/-}$	*junAA*	*mkk7*$^{+/-}$	*mkk7*$^{-/-}$	*junAA*	*mkk7*$^{+/-}$	*mkk7*$^{-/-}$	*junAA*	*c-jun*$^{-/-}$
G1 (%)	66.5	70.2	64.0	65.0	56.3	66.9	65.4	64.8	64.6	62.9
S (%)	14.7	11.8	14.5	16.3	13.0	5.8	14.9	9.0	6.4	7.9
G2/M (%)	18.8	18.0	21.5	18.7	**30.3**	**27.3**	19.7	**26.2**	**29.0**	**29.2**

Cells were stained with PI, and cycle profiles were determined in *mkk7*$^{+/-}$, *mkk7*$^{-/-}$, *mkk7*$^{-/-}$, *c-jun*$^{-/-}$ and *c-junAA* MEFs at the indicated passage numbers. Data from one representative experiment are shown.

RESULTS

Generation of *mkk7* knockout mice

The *mkk7* gene was targeted, as shown in Supplementary information Fig. S1a. Disruption of the gene was confirmed by southern blot analysis of genomic DNA and Northern blot analysis of total RNA (see Supplementary Information, Fig. S1b, c). *mkk7*$^{+/-}$ mice appear normal, are fertile, and show no obvious defects. However, no *mkk7*$^{-/-}$ mice were found from intercrosses between heterozygous mice (Table 1). Thus, loss of MKK7 results in embryonic lethality.

MKK7 controls embryonic liver development

To determine the gestational time of *mkk7* lethality, we examined embryos from heterozygous intercrosses at different developmental stages. *Mkk7*$^{-/-}$ embryos died between E11.5 and E13.5 (Table 1). All *mkk7*$^{-/-}$ embryos were severely anaemic, but otherwise normal in appearance (Fig. 1b). PECAM-1 staining of endothelial cells and H&E (haematoxylin and eosin) staining of blood islands from E8.5–E10.5 embryos showed that MKK7 expression is not essential for blood-island formation in the yolk sac and vasculogenesis (data not shown).

Histological analysis revealed that the liver anlage form normally in E8.5 and E9.5 *mkk7*$^{+/+}$, *mkk7*$^{+/-}$, and *mkk7*$^{-/-}$ embryos (data not shown). However, livers from E11.5 and E12.5 *mkk7*$^{-/-}$ embryos were severely disorganized and contained significantly reduced numbers of parenchymal hepatocytes (Fig. 1d). At E11.5 of embryogenesis, the expression levels of p53, MDM2, phospho-ERKs and phospho-p38 seemed comparable between *mkk7*$^{+/-}$ and *mkk7*$^{-/-}$ livers, as well as in whole embryos (see Supplementary information, Fig. S1d). These data show that MKK7 is essential for liver formation during embryogenesis.

Decreased proliferation and premature senescence in *mkk7*$^{-/-}$ MEFs

As genetic inactivation of *mkk7* resulted in embryonic lethality, we analysed the role of MKK7–JNK signalling in MEFs isolated from *mkk7*$^{+/+}$, *mkk7*$^{+/-}$ and *mkk7*$^{-/-}$ embryos. As predicted from other stud-

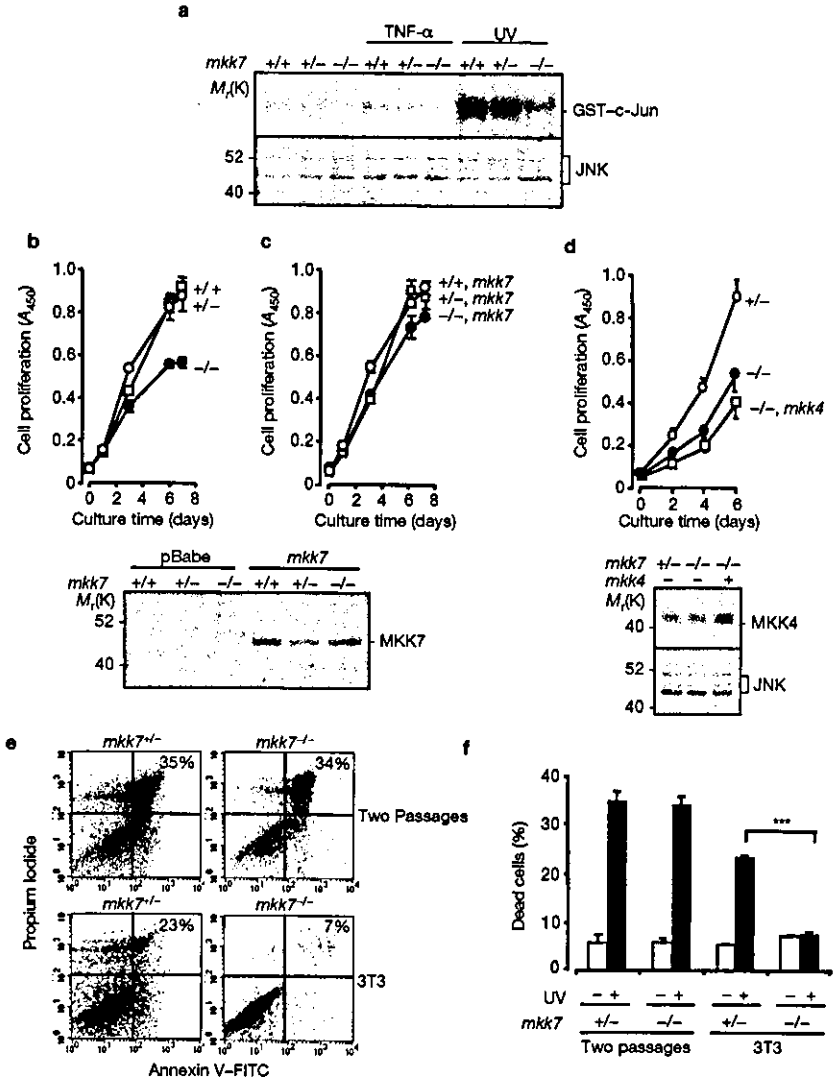

Figure 2 Decreased proliferation and premature senescence of *mkk7*$^{-/-}$ MEFs. (**a**) JNK activity in serum-starved (0.5% serum for 3 days) *mkk7*$^{+/+}$, *mkk7*$^{+/-}$ and *mkk7*$^{-/-}$ MEFs (passage 3) stimulated with TNF-α (10 ng ml^{-1}) and UV (10 J m^{-2}). JNK activity was determined by immune-complex kinase assay using GST–c-Jun as a substrate. (**b–d**) Decreased proliferation of *mkk7*$^{-/-}$ MEFs (passage 4; **b**), and reversal of the proliferation defect by ectopic expression of wild-type MKK7 (**c**), but not by over-expression of wild-type MKK4 (**d**). pBabe (control, **b**), pBabe-MKK7 (**c**) and pBabe-MKK4 (**d**) were introduced into MEFs, and proliferation was determined at the indicated times. Western blots show expression levels of each protein after infection (for the whole blots of **a**, **c** and **d**, see Supplementary information, Fig. S2c–e). In **b**, $P < 0.01$ between *mkk7*$^{+/+}$ or *mkk7*$^{+/-}$ and *mkk7*$^{-/-}$ MEFs (Students *t*-test). (**e**, **f**) Apoptosis in *mkk7*$^{+/-}$ and *mkk7*$^{-/-}$ MEFs. Passage-2 MEFs and 3T3 MEFs were left untreated or were irradiated with 10 J m^{-2} UV 24 h before determination of cell death by annexinV/PI staining. Quantification of three different assays (**f**) and typical annexinV/PI FACS profiles of UV-irradiated MEFs (**e**) are shown. ***$P < 0.001$ between UV-treated *mkk7*$^{+/-}$ and *mkk7*$^{-/-}$ MEFs (Student's *t*-test). In all figures, error bars are shown as standard error of the mean (s.e.m.).

ies[15], loss of MKK7 expression resulted in impaired JNK activation in MEFs at the basal level and after stimulation with tumour necrosis factor α (TNF-α) or UV irradiation (Fig. 2a). Activation and expression of p38-MAPK in MEFs were unaffected in *mkk7*$^{-/-}$ MEFs (data not shown). During the first three passages, cell proliferation was comparable between *mkk7*$^{+/+}$, *mkk7*$^{+/-}$ and *mkk7*$^{-/-}$ MEFs (data not shown). From passages 4–5 onwards, all *mkk7*$^{-/-}$ MEFs analysed showed significantly reduced proliferation under baseline culture conditions (Fig. 2b) and after serum stimulation (data not shown). In all experiments, *mkk7*$^{+/-}$ MEFs behaved similarly to *mkk7*$^{+/+}$ MEFs. Re-expression of wild-type MKK7 (Fig. 2c) restored the reduced proliferation of *mkk7*$^{-/-}$ MEFs to levels observed in wild-type MEFs. Consistent with recent data showing that both MKK4 and MKK7 are required to synergistically activate JNKs[8–10], overexpression of the second JNK activating kinase, MKK4, could not substitute for the loss of MKK7 (Fig. 2d).

To test whether the reduced proliferation in *mkk7*$^{-/-}$ MEFs was

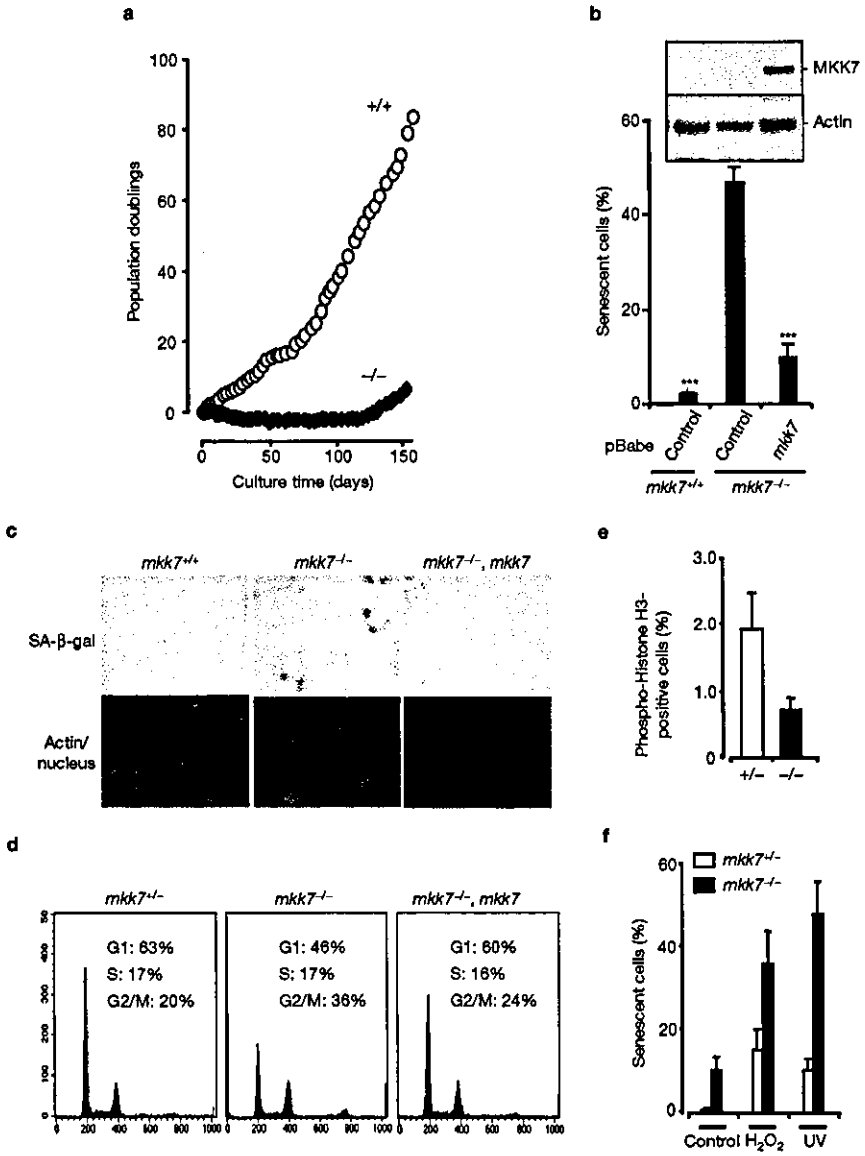

Figure 3 MKK7 is required to protect cells from premature senescence. (**a**) Typical growth curves of *mkk7*$^{+/+}$ and *mkk7*$^{-/-}$ MEFs. One representative experiment out of five is shown. (**b**) Senescence in *mkk7*$^{+/+}$ and *mkk7*$^{-/-}$ MEFs infected with empty pBabe vector (controls) or wild-type MKK7. Senescence was determined at passage 5 by SA-β-galactosidase staining. Western blots show expression levels of each protein after infection (for whole blots, see Supplementary Information, Fig. S2f). ***$P < 0.001$ versus *mkk7*$^{-/-}$ MEFs infected with control pBabe. (**c**) Microscopic analysis of *mkk7*$^{+/+}$, *mkk7*$^{-/-}$ and *mkk7*$^{-/-}$ MEFs expressing wild-type MKK7. SA-β-galactosidase staining (SA-β-gal) is shown in top panels. In the bottom panels, phalloidin–rhodamine (red) was used to stain actin and DAPI (blue) was used to stain nuclei. Representative data from passage-5 cells are shown. Note the flattened and rounded shapes of *mkk7*$^{-/-}$ fibroblasts characteristic of senescent cells. (**d**) Increased G2/M boundaries in *mkk7*$^{-/-}$ MEFs (passage 5) that can be rescued by ectopic expression of wild-type MKK7, but not kinase-dead MKK7 (data not shown). Typical PI FACS analysis is shown for passage-5 MEFs. Some of the *mkk7*$^{-/-}$ cells seem to have greater than 4N DNA content, although this is not a consistent result. (**e**) Numbers of phosphorylated Histone H3-positive cells in *mkk*$^{+/-}$ and *mkk7*$^{-/-}$ MEFs (passage 5) using phospho-specific anti-Histone H3 (Ser10) antibodies. Mean values from three independent experiments are shown. (**f**) *mkk7*$^{+/-}$ and *mkk7*$^{-/-}$ MEFs (passage 3) were UV-irradiated (10 J m^{-2}) or treated with H_2O_2 (150 μM). Stress-induced senescence (mean numbers of SA-β-galactosidase-positive cells) was determined 3 days after stress. The senescent phenotype was confirmed by examination of cell morphology. In addition, increased numbers of cells at the G2/M boundary were observed in those cells (data not shown).

caused by cell-cycle arrest and/or enhanced apoptosis, we first analysed the susceptibility of *mkk7*$^{-/-}$ and *mkk7*$^{+/-}$ MEFs to death stimuli. In particular, it has been shown previously that inactivation of the JNK pathway in MEFs results in resistance to UV-induced cell death[16,17]. Early passage *mkk7*$^{+/-}$ and *mkk7*$^{-/-}$ MEFs showed comparable levels and kinetics of cell death in response to UV- or γ-irradiation (Fig. 2e, f

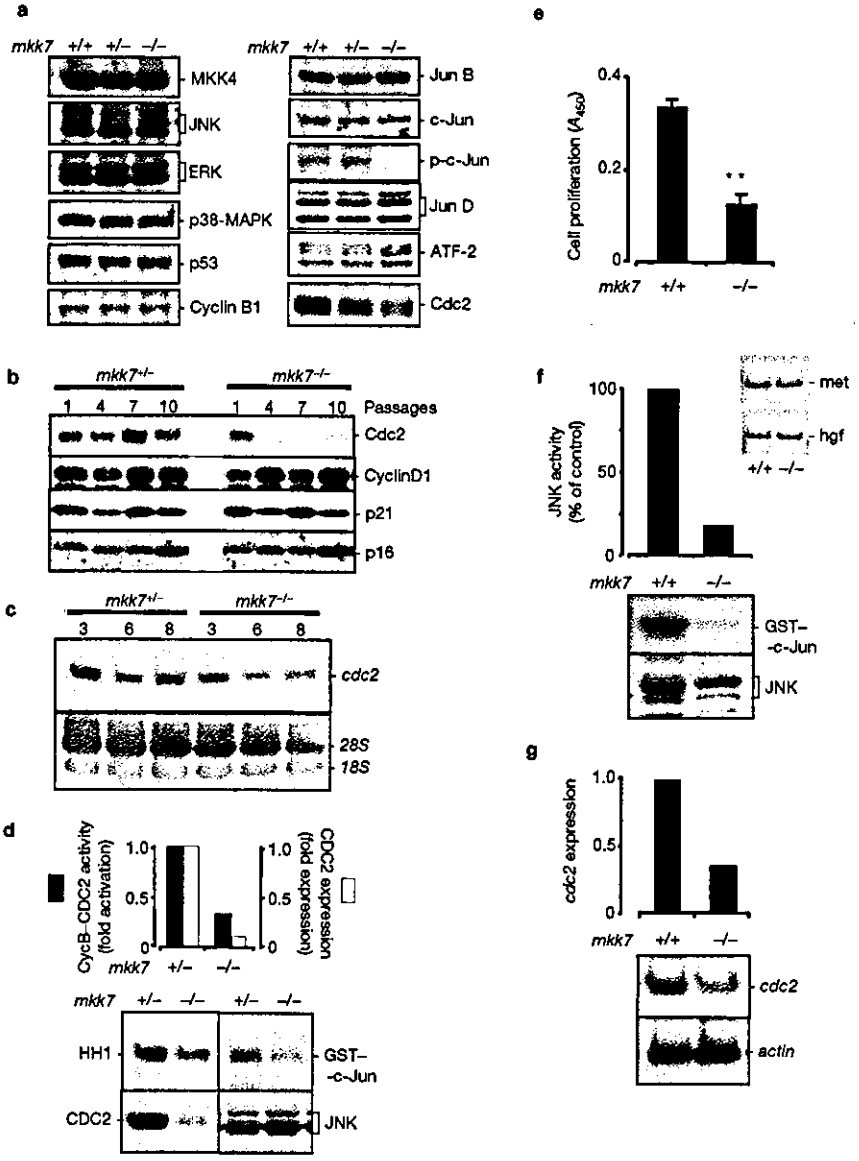

Figure 4 Loss of MKK7 results in decreased CDC2 expression and reduced CDC2 kinase activity. (**a**) Expression levels of the indicated signalling and cell cycle molecules were determined by western blotting of passage-4 *mkk7*$^{+/+}$, *mkk7*$^{+/-}$ and *mkk7*$^{-/-}$ MEFs under normal culture conditions. (**b**) Expression levels of CDC2, cyclinD1, p16 and p21 in passage-1, -4, -7 and -10 *mkk7*$^{+/-}$ and *mkk7*$^{-/-}$ MEFs. (**c**) Reduced expression level of *cdc2* mRNA in *mkk7*$^{-/-}$ MEFs (passage 3, 6 and 8). Total RNA, stained with methylene blue, is shown in the lower panel. (**d**) Decreased cyclin B1–CDC2 complex kinase activity in *mkk7*$^{-/-}$ MEFs (passage 5). CDC2 kinase and JNK activities were determined using Histone H1 (HH1) and GST–c-Jun as substrates. (**e**) Proliferation of embryonic hepatocytes (3×10^3 cells per well) isolated from E11.5 *mkk7*$^{+/-}$ and *mkk7*$^{-/-}$ littermate embryos. $^{**}P < 0.01$. (**f**) Impaired JNK activation in hepatocytes purified from E11.5 *mkk7*$^{-/-}$ embryos. Hepatocytes were stimulated with HGF (30 ng ml^{-1}) for 15 min and then JNK activity was determined by immune-complex kinase assays. Insets show normal levels of *c-Met* and *HGF* mRNA expression in *mkk7*$^{-/-}$ liver cells. (**g**) Decreased expression of *cdc2* mRNA in hepatocytes from E11.5 *mkk7*$^{-/-}$ embryos. Embryonic hepatocytes were isolated as in **e** and quantitative RT–PCR was performed with α-^{32}P-dCTP. PCR products were detected with a phosphoimager. For the whole blots of **a–d**, **f** and **g**, see Supplementary Information, Figs S3a–d and 4a, b.

and not shown). Moreover, spontaneous cell death was comparable between the two genotypes at early passages. However, at later times of culture, *mkk7*$^{-/-}$ 3T3 cells showed resistance to UV-irradiation induced cell death (Fig. 2e, f). Our results indicate that the 'history' and passage number of cells is a critical determinant for cell death susceptibility in the absence of MKK7 expression. Importantly, our data show that

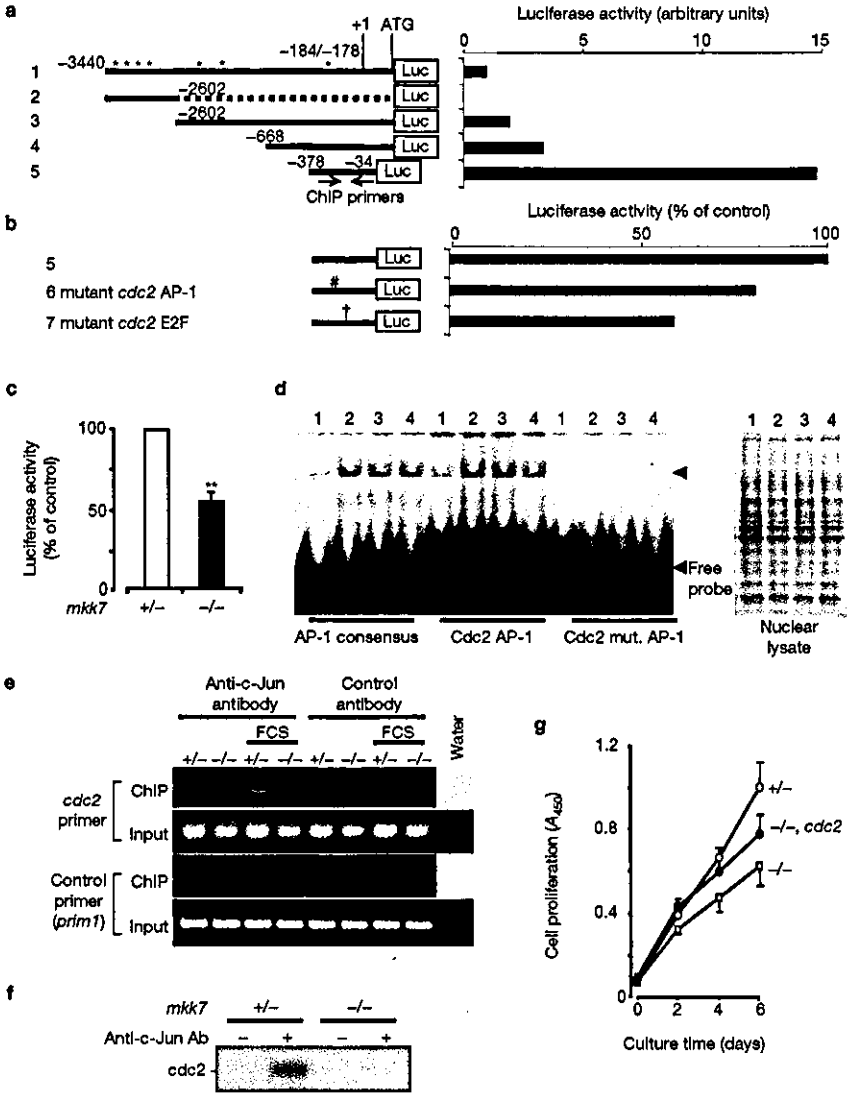

Figure 5 MKK7 controls *cdc2* promoter activity. (**a**, **b**) MKK7 enhances *cdc2* promoter activity in luciferase reporter assays. The indicated constructs were transfected into phoenix E cells and luciferase activities were measured. Potential AP-1-binding sites based on *in silico* analysis are indicated with an asterisk. E2F and *cdc2* AP-1 mutations are indicated as # and †, respectively. Mean values of three experiments are shown. (**c**) Luciferase reporter assays in *mkk7*$^{+/-}$ *and mkk7*$^{-/-}$ MEFs (passage 4). Construct 5 in **a** was used to determine *cdc2* promoter activity. One representative experiment is shown. $^{**}P < 0.01$ between *mkk7*$^{+/-}$ and *mkk7*$^{-/-}$ MEFs. (**d**) Cell extracts were obtained from wild-type MEFs, and EMSAs were performed using consensus AP-1, wild-type *cdc2* AP-1, and mutant *cdc2* AP-1 oligonucleotides. Lane 1, 0.5% serum-starved cells; lane 2, exponentially proliferating cells; lane 3, 20% serum stimulation (30 min); lane 4, 10 J m^{-2} UV stimulation. The right panel shows the amounts of nuclear lysates as loading controls. (**e**, **f**) ChIP assay of c-Jun bound to the *cdc2* AP-1 site in *mkk7*$^{+/-}$and *mkk7*$^{-/-}$ MEFs (passage 4). The positions of the ChIP primers are shown in **a**. The primers for *prim1* gene, which is located on the same chromosome as *cdc2* and does not contain AP-1 consensus sequences in its promoter locus, were used as control. Input indicates total cell lysates before immunoprecipitation to ensure equal loading. ChIP PCR products were visualized using ethidium bromide staining (**e**) or α-^{32}P-dCTP incorporation (**f**). (**g**) Ectopic expression of wild-type CDC2 partially restores the decreased proliferation of passage-4 *mkk7*$^{-/-}$ MEFs. Mean proliferation values of three experiments are shown.

reduced proliferation of *mkk7*$^{-/-}$ MEFs is not the result of increased cell death.

To determine the role of MKK7 in cell proliferation, MEFs were cultured for over 150 days. Similarly to our proliferation data, *mkk7*$^{-/-}$ MEFs did not show any significant differences in population doubling within the first three passages (Fig. 3a). However, during subsequent passages, loss of MKK7 resulted in a marked decrease in cell numbers (Fig. 3a). In all MEF cell lines (five independent cultures) analysed, loss

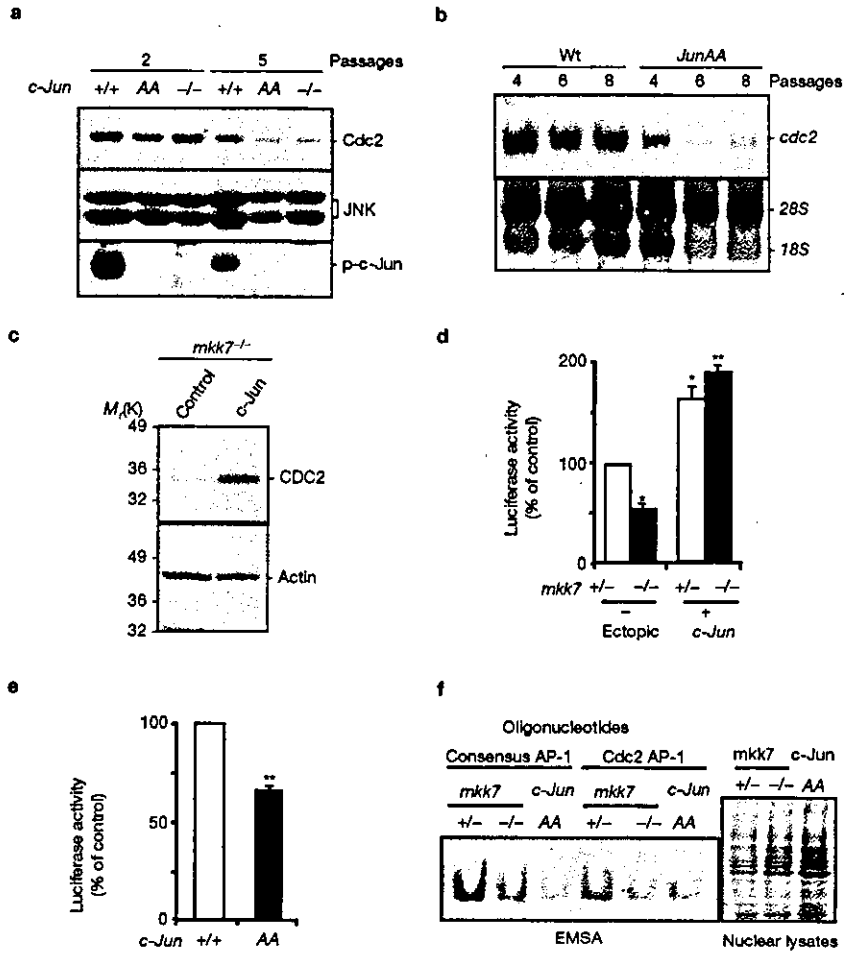

Figure 6 c-Jun regulates CDC2 expression. (**a**) Expression levels of CDC2 protein, JNK and phospho-c-Jun in passage-2 and -5 *c-jun*$^{-/-}$ and *c-junAA* MEFs. (**b**) Expression levels of *cdc2* mRNA in passage-4, -6 and -8 wild-type and *c-junAA* MEFs. Total RNA, stained with methylene blue, is also shown (bottom). (**c**) Overexpression of c-Jun upregulates CDC2. pBabe (control) or pBabe-c-Jun were introduced into *mkk7*$^{-/-}$ MEFs and CDC2 protein expression was determined by western blotting. For the whole blots of **a**–**c**, see Supplementary Information Fig. S4c–e. (**d**) Luciferase reporter assays in *mkk7*$^{+/-}$ *and mkk7*$^{-/-}$ MEFs in the presence and absence of overexpressed c-Jun (passage 4). pBabe-c-Jun or pBabe were introduced in MEFs and construct 5 from Fig. 5a was used to determine *cdc2* promoter activity. $^{*}P < 0.05$, $^{**}P < 0.01$ versus *mkk7*$^{+/-}$ MEFs transfected with control pBabe. (**e**) Luciferase reporter assays of *cdc2* promoter activity in c-*junAA* MEFs. $^{**}P < 0.01$ between *c-JunAA* and wild-type control MEFs. (**f**) EMSA assay in *mkk7*$^{+/-}$, *mkk7*$^{-/-}$ and *c-JunAA* MEF cell extracts using consensus AP-1 and *cdc2* AP-1. The right panel shows loading of nuclear lysates.

of MKK7 resulted in extended crisis and premature senescence, as determined by senescence-associated β-galactosidase (SA-β-gal) staining (Fig. 3b and top panel in Fig. 3c) and an enlarged and flattened cell morphology (Fig. 3c, bottom), both of which are established features of senescence in MEFs[18]. Ectopic expression of wild-type MKK7, but not kinase-dead MKK7, rescued premature senescence in *mkk7*$^{-/-}$ MEFs (Fig. 3b, c, and data not shown). Overexpression of MKK7 also increased proliferation and delayed the onset of crisis and senescence in wild-type MEFs (data not shown). Moreover, genetic inactivation of MKK4 in MEFs resulted in reduced proliferation doubling times and premature senescence, indicating that both MKK4 and MKK7 are essential for these cellular processes (data not shown). These results are consistent with previous data showing that loss of JNK1/JNK2 in MEFs results in reduced proliferation[17] and that inactivation of c-Jun in MEFs results in premature senescence and impaired proliferation[19]. Thus, the MKK4–MKK7-regulated JNK signalling pathway is directly responsible for the control of proliferation and cellular senescence.

Defective G2/M cell-cycle progression

As *mkk7*$^{-/-}$ MEFs undergo premature senescence and display reduced proliferation, we analysed the cell-cycle profiles in *mkk7*$^{-/-}$ MEFs after five passages. Surprisingly, whereas senescent cells are normally arrested at the G1 phase[20], *mkk7*$^{-/-}$ MEF lines displayed more G2/M

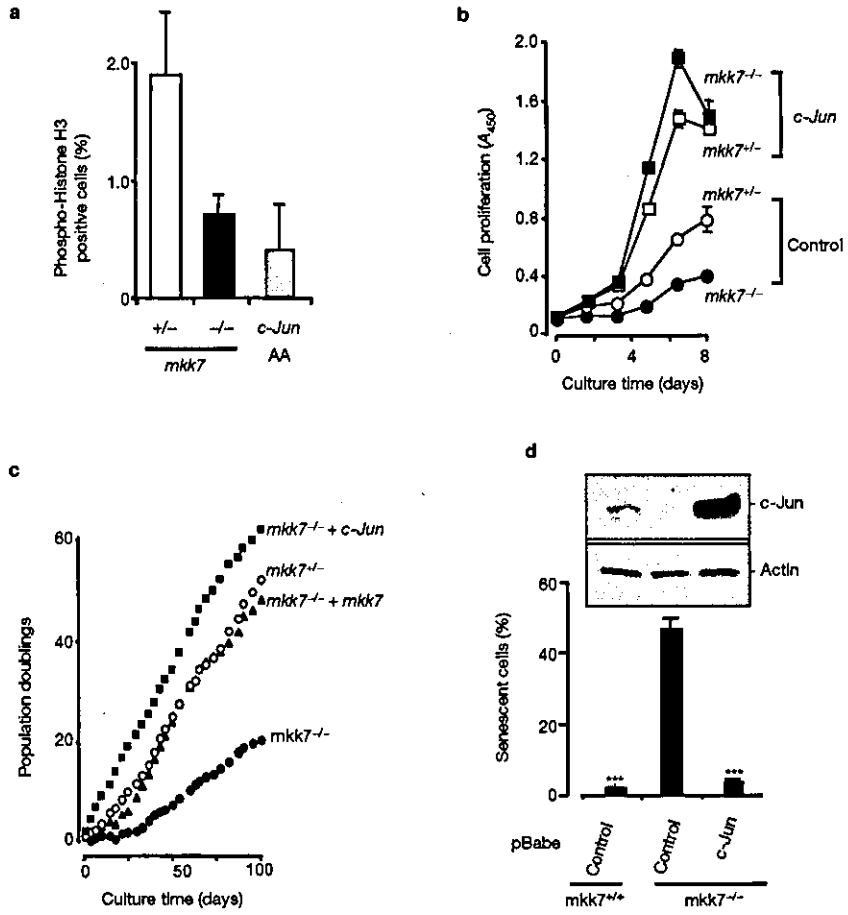

Figure 7 c-Jun rescues senescence and proliferation defects in *mkk7*$^{-/-}$ MEFs. (**a**) Phospho-Histone H3-positive cells in *mkk7*$^{+/-}$, *mkk7*$^{-/-}$ and *c-JunAA* MEFs. Mean values from three independent experiments are shown. (**b**) Cell proliferation (passage 4) was determined at the indicated times. pBabe (control) or pBabe-c-Jun was introduced into *mkk7*$^{+/-}$ and *mkk7*$^{-/-}$ MEFs. (**c**) Growth curves of *mkk7*$^{+/-}$ and *mkk7*$^{-/-}$ MEFs. pBabe (control), pBabe-c-Jun or pBabe-MKK7 were introduced into *mkk7*$^{+/-}$ and *mkk7*$^{-/-}$ MEFs and population doublings were determined as in Fig. 3a. (**d**) c-Jun overexpression rescues cellular senescence of *mkk7*$^{-/-}$ MEFs. Senescence was determined at passage 5 by SA-β-galactosidase staining. Western blots show expression levels of c-Jun and β-actin (for whole blots, see Supplementary Information Fig. S4f). ***$P < 0.001$ versus *mkk7*$^{-/-}$ MEFs.

boundaries when compared with *mkk7*$^{+/-}$ (Fig. 3d) or wild-type (data not shown) MEFs. Re-expression of MKK7 in *mkk7*$^{-/-}$ MEFs abolished the G2/M cell-cycle arrest (Fig. 3d). Synchronized *mkk7*$^{-/-}$ MEFs did not show an apparent defect in G1-to-S-phase entry; however, *mkk7*$^{-/-}$ MEFs displayed an extended G2/M phase after serum stimulation (data not shown). To address whether *mkk7*-deficient MEFs are arrested in G2 or M phase, phospho-Histone H3 staining was performed. Histone H3 is phosphorylated at Ser 10 during M phase, but not at G2 (refs 21, 22). *mkk7*$^{-/-}$ MEFs showed less phospho-Histone H3-positive cells than *mkk7*$^{+/-}$ cells (Fig. 3e), indicating that *mkk7*$^{-/-}$ MEFs are arrested in G2 phase rather than M phase. These data show that loss of MKK7 in MEFs results in an unexpected defect in G2/M cell-cycle progression.

Interestingly, environmental stresses, such as UV irradiation and oxidative stress, trigger a G2/M arrest[23–25] and premature senescence[26]. Therefore, low-passage *mkk7*$^{+/-}$ and *mkk7*$^{-/-}$ MEFs were treated with hydrogen peroxide and UV to test the role of the MKK7–JNK in G2/M arrest and senescence in response to these environmental stresses. *mkk7*$^{-/-}$ MEFs displayed more susceptibility to stress-induced premature senescence (Fig. 3f) and G2/M block (see Supplementary Information, Fig. S2a, b). Thus, MKK7 regulates cellular senescence and G2/M progression in response to environmental stress

Impaired CDC2 expression and CDC2 activity in *mkk7*$^{-/-}$ MEFs

To identify the mechanism through which MKK7 regulates proliferation and G2/M cell cycle progression, we examined the expression levels of molecules known to be involved in cell-cycle control and senescence. Expression of ERK1/2, p38-MAPK, MKK4, JNKs, JunB, JunD, and ATF2 were comparable between *mkk7*$^{+/+}$, *mkk7*$^{+/-}$, and *mkk7*$^{-/-}$ MEFs (Fig. 4a). Consistent with the *in vitro* kinase assays showing reduced JNK activation (Fig 2a), phosphorylation and expression of c-Jun were reduced in *mkk7*$^{-/-}$ MEFs (Fig. 4a). Expression of the cell-cycle molecules cyclin B (Fig. 4a), p16, p21, cyclin D1 (Fig. 4b), p27 and cyclin E (data not shown) were comparable between the different genotypes. Similarly to previously results[15], we did not observe obvious changes in

p53 expression (Fig. 4a). Moreover, telomerase activity in *mkk7*$^{-/-}$ MEFs was comparable with MKK7-expressing MEFs (data not shown).

Intriguingly, a marked reduction in the expression of CDC2 protein was observed (Fig. 4a). CDC2 has been shown to be essential for G2/M cell-cycle progression in multiple organisms[27,28]. Reduced expression of CDC2 in *mkk7*$^{-/-}$ MEFs correlated with the numbers of cell passages; CDC2 expression seemed normal at early passages (passage 1–2: normal G2/M phase, proliferation and population doubling), and consistent with the proliferation defect, it was rapidly downregulated thereafter (passage 4–10: G2/M block and reduced proliferation and population doubling; Fig. 4b). Expression levels of cyclin D1, p21, p16 (Fig. 4b), p53, GADD45 and JNK (data not shown) were similar in *mkk7*$^{+/-}$ and *mkk7*$^{-/-}$ MEFs at the different passage numbers examined. *mkk7*$^{-/-}$ MEFs exhibited reduced JNK activation and delayed CDC2 up-regulation after serum stimulation (data not shown). Reduced expression of *cdc2* mRNA was also observed in *mkk7*$^{-/-}$ MEFs (Fig. 4c). Importantly, cyclin B1-associated CDC2 kinase activity was markedly reduced in *mkk7*$^{-/-}$ MEFs (Fig. 4d), indicating that reduced CDC2 expression correlates with impaired cyclin B1/CDC2 activity. These data suggest that CDC2 is a potential molecular target for MKK7 regulated stress kinase signalling.

Impaired proliferation and CDC2 expression in primary *mkk7*$^{-/-}$ hepatocytes

Whereas hepatogenesis seemed normal at earlier stages of embryogenesis in *mkk7*$^{-/-}$ embryos, mutation of MKK7 results in embryonic lethality that correlated with impaired liver development (Fig. 1). The defective development of the parenchymal liver in *mkk7*$^{-/-}$ embryos seemed to parallel our results in *mkk7*-null MEFs, which display normal proliferation at initial passages that is rapidly followed by a proliferation defect. Therefore, proliferation was analysed in hepatocytes and haematopoietic liver progenitor cells from E11.5 *mkk7*$^{-/-}$ embryos. Haematopoietic precursor cells from both *mkk7*$^{+/-}$ and *mkk7*$^{-/-}$ embryos stained positive for 5-bromo-2'-deoxyuridine (BrdU) labelling *in vivo*, indicating that these cells were proliferating (data not shown). In addition, using *in vitro* clonal differentiation assays[11], *mkk7*$^{-/-}$ and *mkk7*$^{+/-}$ precursors derived from the liver of E10.5 embryos developed into macrophages/monocytes, mast cells and immunoglobulin-secreting B lymphocytes (data not shown). Thus, haematopoietic precursors present in *mkk7*$^{-/-}$ liver remnants can give rise to various haematopoietic cell lineages. In contrast, proliferation of hepatocytes was markedly impaired in E11.5 *mkk7*$^{-/-}$ embryos, as determined by BrdU *in vivo* labelling (data not shown). Reduced proliferation of hepatocytes was also observed in primary hepatocyte cultures isolated from *mkk7*$^{-/-}$ E11.5 embryos (Fig. 4e). JNK activation was abolished in these primary *mkk7*$^{-/-}$ hepatocytes in response to hepatocyte growth factor (HGF) treatment (Fig. 4f). Similarly to *mkk7*$^{-/-}$ MEFs, *cdc2* mRNA expression was downregulated in primary *mkk7*$^{-/-}$ hepatocytes (Fig. 4g). Thus, these results suggest that the MKK7–JNK signalling pathway is important for CDC2 expression, and proliferation of MEFs and primary hepatocytes.

CDC2 is a target for MKK7–JNK signalling

Reduced CDC2 expression in *mkk7*$^{-/-}$ MEFs could be an indirect consequence of premature senescence, or CDC2 could be a direct target of the MKK7–JNK signalling pathway. MKK7 or JNK was not co-immunopreciptated with CDC2/ cyclin B1 and phosphorylation of CDC2/ cyclin B1 by recombinant MKK7 or recombinant JNK was not observed using *in vitro* kinase assays (data not shown). *In silico* analysis of the murine *cdc2* promoter region identified several predicted AP-1 elements in the −3,440 to +1 bp region (Fig. 5a, asterisks). Luciferase promoter assays using deletion mutants in phoenixE cells showed that the sequence 5'-AGAGTCA-3' at −184/−178 of the *cdc2* promoter is a potential AP-1 site required for effective *cdc2* transactivation (Fig. 5a). It should be noted that the identical promoter sequence has been previously identified in the prostaglandin G/H synthase-2 promoter[29]. Treatment with TPA (12-*O*-tetradecanoylphorbol-13-acetate) and serum induce binding to oligonucleotides containing the 5'-AGAGTCA-3' sequence, and antibodies specific for c-Jun and c-Fos inhibit binding of AP-1 to the prostaglandin G/H synthase-2 promoter in electromobility shift assays (EMSAs) [29]. Mutation of the *cdc2* AP-1 site rendered lower promoter transactivation in our luciferase assays, albeit to a lesser extent than a mutation in the previously defined[30] *cdc2* promoter −129/−121 E2F-binding site (Fig. 5b). Whether additional AP-1 sites are critical in the CDC2 promoter remains to be determined. Furthermore, transactivation of a *cdc2*-promoter–luciferase reporter construct was impaired in *mkk7*$^{-/-}$ MEFs (Fig. 5c).

In EMSA assays (Fig. 5d), both the consensus AP-1 site and the 5'-AGAGTCA-3' AP-1 site present in the cdc2 promoter showed band shifts after incubation in serum and UV stimulation. Mutation of the −184/−178 *cdc2* AP-1 site abolished the band shift (Fig. 5d). To determine whether c-Jun, the downstream target of MKK7–JNK, can bind to the *cdc2* promoter region under physiological conditions, chromatin immunoprecipitation (ChIP) analysis was performed (Fig. 5e). The *cdc2* promoter region encompassing the −184/−178 AP-1 site was precipitated in the presence of an anti-c-Jun specific antibody, indicating that c-Jun can bind to the *cdc2* promoter but does not bind to the control *prim1* gene promoter region present on the same chromosome (Fig. 5e). Binding of c-Jun to the *cdc2* promoter in ChIP experiments was confirmed by radioactive PCR (Fig. 5f). To test whether CDC2 is important for cell proliferation in *mkk7*$^{-/-}$ MEFs, wild-type CDC2 was over-expressed. Ectopic expression of wild-type CDC2 in *mkk7*$^{-/-}$ MEFs partially restored proliferation (Fig. 5g). These data identify CDC2 as a target of the MKK7–JNK signalling pathway and indicate that CDC2 might be important for overcoming the cell cycle block of *mkk7*-null cells. However, we cannot rule out the possibility that CDC2 expression might also be controlled indirectly by other MKK7–JNK–c-Jun-regulated molecules, as the direct effect of c-Jun on *cdc2* promoter activity is not strong.

Control of CDC2 expression, senescence and G2/M progression by c-Jun

The MKK7–JNK stress pathway regulates gene transcription through phosphorylation of multiple transcription factors, including c-Jun or ELK-1 (refs 1–5). As we observed reduced phosphorylation and expression of c-Jun in *mkk7*$^{-/-}$ fibroblasts (Fig. 4a), and c-Jun controls the *cdc2* promoter (Fig. 5), we wanted to confirm the role of c-Jun in cellular senescence, G2/M progression and CDC2 expression in genetic experiments.

Consistent with the impaired phosphorylation of c-Jun and reduced CDC2 expression in *mkk7*$^{-/-}$ MEFs, *c-jun*$^{-/-}$ MEFs also displayed reduced expression of CDC2 protein at later passages (Fig. 6a). Importantly, MEFs derived from *c-junAA* mutant mice carrying a mutant of both c-Jun phosphorylation sites[13,14] also showed reduced CDC2 protein (Fig. 6a), as well as reduced *cdc2* mRNA expression after more than five passages (Fig. 6b). Over-expression of c-Jun in *mkk7*$^{-/-}$ MEFs restored CDC2 expression (Fig. 6c) and transactivation of the *cdc2* AP-1 promoter construct to levels observed in wild-type MEFs (Fig. 6d). Activity of the *cdc2* promoter construct was also reduced in *c-junAA* MEFs (Fig. 6e). Moreover, in EMSA experiments binding of MEF extracts to consensus AP-1 and *cdc2* AP-1 oligonucleotides were reduced in both *mkk7*$^{-/-}$ and *c-junAA* MEFs (Fig. 6f). These data show

that CDC2 expression can be regulated by the MKK7–JNK–c-Jun signalling pathway.

To evaluate whether c-Jun controls G2/M progression, cell-cycle analysis was performed in early passage *c-jun*$^{-/-}$ and *c-junAA* MEFs. Similarly to *mkk7*$^{-/-}$ MEFs, loss of c-Jun or inactivation of the JNK phosphorylation sites of c-Jun resulted in the accumulation of cells at the G2/M boundaries beginning from passage 4 (Table 2). Immunostaining with phospho-Histone H3 confirmed that the arrest occurred at the G2 phase, rather than the M phase (Fig. 7a). Importantly, over-expression of c-Jun rescued the defects in proliferation and premature senescence observed in *mkk7*$^{-/-}$ MEFs (Fig. 7b–d). These data suggest an involvement of the MKK7–JNK–c-Jun pathway in G2/M cell cycle progression and cell proliferation in MEFs.

DISCUSSION

Our results show that MKK7 and c-Jun are critical for MEF proliferation and G2/M cell-cycle progression. Previous data from other groups have shown that the JNK–c-Jun signalling pathway is required to promote proliferation in primary MEFs[17,19,32]. However, it has been shown recently that JNK1/JNK2 signalling may attenuate proliferation after Ras-mediated transformation in 3T3 cells[32]. It should be noted that overexpression of Ras causes premature cellular senescence in primary MEFs, whereas it can transform most immortalized cells (such as 3T3 MEFs) in the presence of inactive tumour suppressors such as p53 or p16 (ref. 33) during long-term cell culture. Thus, the different genetic background and treatments might determine the different outcomes. Our genetic and biochemical data clearly show that in non-transformed primary MEFs, as well as embryonic liver cells, MKK7 is a crucial kinase for cell proliferation. In contrast, it has been shown that MKK7 is a negative regulator of haematopoietic cell proliferation[12,34]. The *in vitro* growth behaviours of haematopoietic cells are different from other cell types, and the role of MKK7–JNK in haematopoietic cells has only been studied under basal conditions. Thus, it would be interesting to determine the growth behaviours of such cells under conditions of stress, such as low population densities or altered serum condition. In addition, it is possible that MKK7 might regulate additional pathways.

One intriguing aspect of our results is that early passage *mkk7*$^{-/-}$ MEFs behave similarly to wild-type cells, but then rapidly down-regulate CDC2 expression and display premature senescence and defective proliferation. Similarly, proliferation of primary hepatocytes in *mkk7*$^{-/-}$ embryos seems to be normal in early foetal development, followed by downregulation of CDC2 and defective proliferation. In cell culture, it has been shown that conditions of stress, such as low serum or low cell densities, trigger premature senescence in wild-type fibroblasts and many other cell types[35]. Thus, it seems that under conditions of environmental stress and possibly during certain developmental processes such as liver formation, the MKK7–JNK–c-Jun pathway might function to upregulate CDC2 expression and maintain the proliferative state of the cells. Determination of cell fates by MKK7–JNK–c-Jun-induced CDC2 expression might explain why loss of MKK7 results in premature senescence and a G2/M cycle arrest, whereas the cells that express MKK7 undergo crisis at much later stages and predominantly arrest at G1 phase. Our results provide a molecular link between environmental stresses, premature senescence and G2/M cell-cycle progression. Whether MKK7–JNK-c-Jun signalling is involved in the regulation of molecules previously known to be involved in senescence needs to be determined. To investigate the connection to p53 (ref. 36) further, we generated *p53*$^{-/-}$*mkk7*$^{-/-}$ MEFs and observed rescue of CDC2 expression and cellular senescence, as well as restored proliferation. Thus, p53 is also important for the process. In addition, some other molecules controlled by the MKK7–JNK–c-Jun pathway might also be involved in the regulation of CDC2 expression at transcriptional, translational and post-translational levels, as it has been shown that *cdc2* transactivation is regulated by multiple mechanisms depending on cell types[37] and that c-Jun can control a variety of molecules such as E2F[19].

It has been suggested that the mechanisms regulating the cell cycle also have a role in apoptosis[38]. The induction of proteins that control G1/S transition in proliferating cells occurs in dying neurons[39], and G1 cyclin-dependent kinases seem to trigger neuronal cell death[40]. Moreover, E2F1-1 and CDK2 seem to control thymocyte apoptosis[41,42]. The G2/M cell-cycle regulator CDC2 induces phosphorylation of the BH3-only protein BAD and triggers neuronal apoptosis[43]. This notion is consistent with our results on the normal susceptibility to cell death in CDC2-expressing *mkk7*$^{-/-}$ MEFs, but the resistance to death triggers in *mkk7*$^{-/-}$ 3T3 cells that express low levels of CDC2. Furthermore, we showed that overexpression of constitutively active CDC2 in wild-type and *mkk7*$^{-/-}$ MEFs results in cell death (data not shown). Thus, regulation of CDC2 by stress kinases might be also involved in stress-kinase-regulated cell death. The role of JNKs in cell death has been controversial and is dependent on the experimental system used. Our results in MEF apoptosis experiments indicate that the MKK7–JNK–c-Jun pathway determines the molecular history of cells, and this is a critical determinant for cell death. Whether stress kinases also set the molecular switches for cell death susceptibility in other cell types remains to be determined.

Our results show that MKK7 is essential for embryogenesis and liver development. Loss of MKK7 in fibroblasts results in impaired proliferation, premature senescence and a G/2M cell-cycle arrest. We identified the G2/M kinase CDC2 as a molecular target for the MKK7–JNK–c-Jun signalling pathway. These data provide a new paradigm by which the MKK7–JNK–c-Jun signalling pathway couples developmental and environmental cues to proliferation, G2/M cycle arrest and cellular senescence. □

METHODS

Gene targeting. To disrupt the murine *mkk7* gene in embryonic stem cells, a portion of exon 9, including the phosphorylation motif, was replaced with a PGK-Neo cassette (see Supplementary information, Fig. S1a), as described previously[34]. *c-Jun* and *c-JunAA* mutant mice and MEFs have been described previously[13,19]. All mice were kept at the Ontario Cancer Institute and IMP animal facilities in accordance with institutional guidelines.

MEF and hepatocyte cultures. MEFs were prepared from E11.5 embryos and maintained in DMEM contatining 10% foetal calf serum (FCS). Cell proliferation in all MEFs was determined using WST-1 (Roche, Indianapolis, IN). The percentage of cells in each phase of the cell cycle was calculated with ModiFit software (Becton Dickinson, Oakville, Canada). Population doubling curves were determined using trypan-blue exclusion. For detection of apoptosis, MEFs were stained with annexin V/propidium iodide (PI) using an apoptosis detection kit (R&D Systems, Minneapolis, MN). For cell-cycle analysis, MEFs were fixed with 70% ethanol, labelled with PI and analysed by FACS. All samples were analysed by flow cytometry. Protein expression levels were determined using antibodies specific to p16, p21, cyclin D1, cyclin B1, MKK4, JNKs, p38-MAPK, ATF2, c-Jun, phospho-c-Jun, JunB, JunD (antibodies were purchased from Santa Cruz Biotechnology, Santa Cruz, CA), p53 (Novacastra, distributed by Vecter Laboratories, Burlingame, CA), CDC2 and ERK1/2 (Cell Signaling, Beverly, MA). For primary hepatocyte cultures, haematopoietic cells were depleted using antibodies to CD45 and TER119. The remaining parenchymal liver cells were cultured for 2 days, and cell proliferation was determined using WST-1 (Roche). *cdc2* mRNA expression was detected with a full-length CDC2 cDNA probe or RT-PCR. JNK activity in mouse embryonic liver was determined as described[44].

Expression assays. For ectopic gene expression, the retroviral vectors pBabe-puro, pBabe-puro-Flag-MKK7, pBabe-puro-MKK4, pBabe-puro-c-Jun or

pBabe-puro-CDC2 (wild-type) were transfected into a phoenix-E packaging cell line. MEFs were cultured in the supernatant of the packaging cells for 1 day and selected with 2.5 mg ml^{-1} puromycin for 2 days before recovery for a further 2 days. Empty pBabe-puro vectors did not have any detectable effect on the phenotype of MEFs.

Detection of senescent cells and cell staining. SA-β-gal staining was performed using a senescence staining kit (Cell Signaling). For Phalloidin–rhodamine/DAPI staining, SA-β-gal-stained cells were fixed, treated with 0.1% Triton X-100/3% skimmed milk/TBS and double-stained with phalloidin–rhodamine (Sigma, St Louis, MO) and DAPI (Molecular Probes, Eugene, OR). All SA-β-gal-positive cells had the typical flattened cell morphology determined by phalloidin/DAPI staining. Phospho-Histone H3 was determined using a phosphorylation (Ser 10)-specific antibody (Cell Signaling).

Promoter assays. The full-length CDC2 promoter was cloned from mouse genomic DNA using PCR, and the sequence was confirmed. The promoter constructs were transfected into Phoenix E cells or *mkk7*$^{+/-}$ and *mkk7*$^{-/-}$ MEFs, and luciferase activity was determined using a Luciferase Assay Kit (Promega, Madison, WI). For EMSAs, cell extracts were harvested from 5×10^6 cells according to standard protocols. Briefly, protein extracts (1 μg) were incubated in 20 μl binding buffer with end-labelled, double-stranded, oligonucleotide probes (consensus AP-1: 5′-CGCTTGATGACTCAGCCGGAA-3′; CDC2 promoter AP-1 site: 5′-AACAGAGCTCAAGAGTCAGTTGG-3′; mutant CDC2 promoter AP1 site: 5′-AACAGAGCTCAAGATCTAGTTGG-3′) and fractionated on a 5% polyacrylamide gel. The binding buffer was: 10 mM Hepes-HCl at pH 7.9, 100 mM potassium chloride, 0.5 mM magnesium chloride, 0.1 mM EDTA, 0.5 mM dithiothreitol, 2 μg poly (dI-dC) and 10% glycerol. Chromatin immunoprecipitations (ChIPs) were performed as described[45]. The sequences of the ChIP primers were 5′-CTGTCACTTTGGTGGCTGGC-3′ and 5′-TCCGACTCACGCCATACCTC-3′ for *cdc2*; 5′-GTCAGCATCTAGCACACAGGTCC-3′ and 5′-GAAATCCAGGTAGGGTTCCAGG-3′ for *prim1*.

Kinase assays. To detect JNK and p38-MAPK activities, JNK proteins were immunoprecipitated at 4 °C using anti-JNK antibodies (C-17; Santa Cruz). Kinase activities were determined using glutathione *S*-transferase (GST)–c-Jun as a substrate in the presence of 50 μM γ-^{32}P-ATP. The amount of total JNK protein in the immunoprecipitated lysates were determined by Western blotting. cyclinB1/CDC2 kinase activities were determined by anti- cyclinB1 immunocomplex kinase assays using Histone H1 (HH1) as substrate.

Note: Supplementary Information is available on the Nature Cell Biology website.

ACKNOWLEDGMENTS

We thank J. Woodgett, L. Harrington, J. C. Zuniga-Pflucker, T. Schmitt, J. Joza, C. Krawczyk, E. Griffith, L. Barra, M. Crackower, U. Erickson, L. Zhang, H. Hara and M. Rangachari for discussion and reagents. T.W. is supported by the H15th fellowship of the Japan Society for the Promotion of Science. This work is supported by the National Cancer Institute of Canada (NCIC), the Institute of Molecular Biotechnology of the Austrian Academy of Sciences (IMBA), and the Jubilaeumsfonds of the Austrian National Bank.

COMPETING FINANCIAL INTERESTS

The authors declare that they have no competing financial interests.

Received 26 June 2003; accepted 28 January 2004
Published online at http://www.nature.com/naturecellbiology.

1. Chang, L. & Karin, M. Mammalian MAP kinase signalling cascades. *Nature* **410**, 37–40 (2001).
2. Seger, R. & Krebs, E. G. The MAPK signaling cascade. *FASEB J.* **9**, 726–735 (1995).
3. Tibbles, L. A. & Woodgett, J. R. The stress-activated protein kinase pathways. *Cell Mol. Life Sci.* **55**, 1230–1254 (1999).
4. Waskiewicz, A. J. & Cooper, J. A. Mitogen and stress response pathways: MAP kinase cascades and phosphatase regulation in mammals and yeast. *Curr. Opin. Cell Biol.* **7**, 798–805 (1995).
5. Davis, R. J. Signal transduction by the JNK group of MAP kinases. *Cell* **103**, 239–252 (2000).
6. Roovers, K. & Assoian, R. K. Integrating the MAP kinase signal into the G1 phase cell cycle machinery. *Bioessays* **22**, 818–826 (2000).
7. Johnson, G. L. & Lapadat, R. Mitogen-activated protein kinase pathways mediated by ERK, JNK, and p38 protein kinases. *Science* **298**, 1911–1912 (2002).
8. Kishimoto, H. *et al.* Different properties of SEK1 and MKK7 in dual phosphorylation of stress-induced activated protein kinase SAPK/JNK in embryonic stem cells. *J. Biol. Chem.* **278**, 16595–16601 (2003).
9. Wada, T. *et al.* Impaired synergistic activation of stress-activated protein kinase SAPK/JNK in mouse embryonic stem cells lacking SEK1/MKK4: different contribution of SEK2/MKK7 isoforms to the synergistic activation. *J. Biol. Chem.* **276**, 30892–30897 (2001).
10. Fleming, Y. *et al.* Synergistic activation of stress-activated protein kinase 1/c-Jun N-terminal kinase (SAPK1/JNK) isoforms by mitogen-activated protein kinase kinase 4 (MKK4) and MKK7. *Biochem J.* **352**, 145–154 (2000).
11. Nishina, H. *et al.* Defective liver formation and liver cell apoptosis in mice lacking the stress signaling kinase SEK1/MKK4. *Development* **126**, 505–516 (1999).
12. Dong, C. *et al.* JNK is required for effector T-cell function but not for T-cell activation. *Nature* **405**, 91–94 (2000).
13. Behrens, A., Sibilia, M. & Wagner, E. F. Amino-terminal phosphorylation of c-Jun regulates stress-induced apoptosis and cellular proliferation. *Nature Genet.* **21**, 326–329 (1999).
14. Behrens, A., Jochum, W., Sibilia, M. & Wagner, E. F. Oncogenic transformation by ras and fos is mediated by c-Jun N-terminal phosphorylation. *Oncogene* **19**, 2657–2663 (2000).
15. Tournier, C. *et al.* MKK7 is an essential component of the JNK signal transduction pathway activated by proinflammatory cytokines. *Genes Dev* **15**, 1419–1426 (2001).
16. Hochedlinger, K., Wagner, E. F. & Sabapathy, K. Differential effects of JNK1 and JNK2 on signal specific induction of apoptosis. *Oncogene* **21**, 2441–2445 (2002).
17. Tournier, C. *et al.* Requirement of JNK for stress-induced activation of the cytochrome *c*-mediated death pathway. *Science* **288**, 870–874 (2000).
18. Dimri, G. P. *et al.* A biomarker that identifies senescent human cells in culture and in aging skin *in vivo*. *Proc. Natl Acad. Sci. USA* **92**, 9363–9367 (1995).
19. Schreiber, M. *et al.* Control of cell cycle progression by c-Jun is p53 dependent. *Genes Dev.* **13**, 607–619 (1999).
20. Sherwood, S. W., Rush, D., Ellsworth, J. L. & Schimke, R. T. Defining cellular senescence in IMR-90 cells: a flow cytometric analysis. *Proc. Natl Acad. Sci. USA* **85**, 9086–9090 (1988).
21. Paulson, J. R., Taylor, S. S., Lake, R. S. & Salzman, N. P. Phosphorylation of histones 1 and 3 and nonhistone high mobility group 14 by an endogenous kinase in HeLa metaphase chromosomes. *J. Biol. Chem.* **257**, 6064–6072 (1982).
22. Lake, R. S. & Salzman, N. P. Occurrence and properties of a chromatin-associated F1-histone phosphokinase in mitotic Chinese hamster cells. *Biochemistry* **11**, 4817–4826 (1972).
23. Bulavin, D. V. *et al.* Initiation of a G2/M checkpoint after ultraviolet radiation requires p38 kinase. *Nature* **411**, 102–107 (2001).
24. Shackelford, R. E., Kaufmann, W. K. & Paules, R. S. Cell cycle control, checkpoint mechanisms, and genotoxic stress. *Environ. Health Perspect.* **107**, 5–24 (1999).
25. Orren, D. K., Petersen, L. N. & Bohr, V. A. A UV-responsive G2 checkpoint in rodent cells. *Mol. Cell. Biol.* **15**, 3722–3730 (1995).
26. Toussaint, O. *et al.* Stress-induced premature senescence. Essence of life, evolution, stress, and aging. *Ann. NY Acad. Sci.* **908**, 85–98 (2000).
27. Th'ng, J. P. *et al.* The FT210 cell line is a mouse G2 phase mutant with a temperature-sensitive CDC2 gene product. *Cell* **63**, 313–324 (1990).
28. Arion, D., Meijer, L., Brizuela, L. & Beach, D. *cdc2* is a component of the M phase-specific histone H1 kinase: evidence for identity with MPF. *Cell* **55**, 371–378 (1988).
29. Okada, Y., Voznesensky, O., Herschman, H., Harrison, J. & Pilbeam, C. Identification of multiple *cis*-acting elements mediating the induction of prostaglandin G/H synthase-2 by phorbol ester in murine osteoblastic cells. *J. Cell. Biochem.***78**, 197–209 (2000).
30. Dalton, S. Cell cycle regulation of the human cdc2 gene. *EMBO J.* **11**, 1797–1804 (1992).
31. Kovary, K. & Bravo, R. The jun and fos protein families are both required for cell cycle progression in fibroblasts. *Mol. Cell. Biol.* **11**, 4466–4472 (1991).
32. Kennedy, N. J. *et al.* Suppression of Ras-stimulated transformation by the JNK signal transduction pathway. *Genes Dev.* **17**, 629–637 (2003).
33. Serrano, M., Lin, A. W., McCurrach, M. E., Beach, D. & Lowe, S. W. Oncogenic ras provokes premature cell senescence associated with accumulation of p53 and p16INK4a. *Cell* **88**, 593–602 (1997).
34. Sasaki, T. *et al.* The stress kinase mitogen-activated protein kinase kinase (MKK)7 is a negative regulator of antigen receptor and growth factor receptor-induced proliferation in hematopoietic cells. *J. Exp. Med.* **194**, 757–768 (2001).
35. Didinsky, J. B. & Rheinwald, J. G. Failure of hydrocortisone or growth factors to influence the senescence of fibroblasts in a new culture system for assessing replicative lifespan. *J. Cell. Physiol.* **109**, 171–179 (1981).
36. Wynford-Thomas, D. p53: guardian of cellular senescence. *J. Pathol.* **180**, 118–121 (1996).
37. Sugarman, J. L., Schonthal, A. H. & Glass, C. K. Identification of a cell-type-specific and E2F-independent mechanism for repression of cdc2 transcription. *Mol. Cell. Biol.* **15**, 3282–3290 (1995).
38. King, K. L. & Cidlowski, J. A. Cell cycle and apoptosis: common pathways to life and death. *J. Cell. Biochem.* **58**, 175–180 (1995).
39. Freeman, R. S., Estus, S. & Johnson, E. M. Jr. Analysis of cell cycle-related gene expression in postmitotic neurons: selective induction of cyclin D1 during programmed cell death. *Neuron* **12**, 343–355 (1994).
40. Park, D. S. *et al.* cyclin-dependent kinases participate in death of neurons evoked

by DNA-damaging agents. *J. Cell Biol.* **143**, 457–467 (1998).
41. Hakem, A., Sasaki, T., Kozieradzki, I. & Penninger, J. M. The cyclin-dependent kinase Cdk2 regulates thymocyte apoptosis. *J. Exp. Med.* **189**, 957–968 (1999).
42. Field, S. J. *et al.* E2F-1 functions in mice to promote apoptosis and suppress proliferation. *Cell* **85**, 549–561 (1996).
43. Konishi, Y., Lehtinen, M., Donovan, N. & Bonni, A. Cdc2 phosphorylation of BAD links the cell cycle to the cell death machinery. *Mol. Cell* **9**, 1005–1016 (2002).
44. Watanabe, T. *et al.* SEK1/MKK4-mediated SAPK/JNK signaling participates in embryonic hepatoblast proliferation via a pathway different from NF-κB-induced anti-apoptosis. *Dev. Biol.* **250**, 332–347 (2002).
45. Weinmann, A. S., Bartley, S. M., Zhang, T., Zhang, M. Q. & Farnham, P. J. Use of chromatin immunoprecipitation to clone novel E2F target promoters. *Mol. Cell Biol.* **21**, 6820–6832 (2001).

Transplantation of Bone Marrow Cells Reduces CCl_4-Induced Liver Fibrosis in Mice

Isao Sakaida,[1] Shuji Terai,[1] Naoki Yamamoto,[1] Koji Aoyama,[1] Tsuyoshi Ishikawa,[1] Hiroshi Nishina,[2] and Kiwamu Okita[1]

We investigated the effect of bone marrow cell (BMC) transplantation on established liver fibrosis. BMCs of green fluorescent protein (GFP) mice were transplanted into 4-week carbon tetrachloride (CCl_4)–treated C57BL6 mice through the tail vein, and the mice were treated for 4 more weeks with CCl_4 (total, 8 weeks). Sirius red and GFP staining clearly indicated migrated BMCs existing along with fibers, with strong expression of matrix metalloproteinase (MMP)-9 shown by anti–MMP-9 antibodies and *in situ* hybridization. Double fluorescent immunohistochemistry showed the expression of MMP-9 on the GFP-positive cell surface. Film *in situ* zymographic analysis revealed strong gelatinolytic activity in the periportal area coinciding with the location of MMP-9–positive BMCs. Four weeks after BMC transplantation, mice had significantly reduced liver fibrosis, as assessed by hydroxyproline content of the livers, compared to that of mice treated with CCl_4 alone. Subpopulation of Liv8-negative BMCs was responsible for this fibrolytic effect. In conclusion, mice with BMC transplants with continuous CCl_4 injection had reduced liver fibrosis and a significantly improved survival rate after BMC transplantation compared with mice treated with CCl_4 alone. This finding introduces a new concept for the therapy of liver fibrosis. *Supplementary material for this article can be found on the HEPATOLOGY website (http://interscience.wiley.com/jpages/0270-9139/suppmat/index.html).* (HEPATOLOGY 2004;40: 1304–1311.)

Recent reports have shown the capacity of the bone marrow cell (BMC) to differentiate into a variety of non-hematopoietic cell lineages.[1–5] These results indicate that the BMC is an attractive cell source for regenerative medicine compared with tissue-specific stem cells.[6] The capacity of the BMC to differentiate into hepatocytes and intestinal cells has been shown by Y-chromosome detection in autopsy analysis of human female recipients of BMCs from male donors.[7,8] Although Lagasse et al. reported that purified hematopoietic stem cells could differentiate into hepatocytes using a fumarylacetate hydrase-deficient model,[5] Wagers et al. showed little evidence of plasticity in adult hematopoietic stem cells.[9] Thus, although there is still controversy about which part of BMCs can differentiate into hepatocytes, the BMC seems to have the plasticity to differentiate into such cells. From the point of view of therapy, one of the targets of liver disease for BMC transplantation is liver cirrhosis with chronic liver failure. This is an unphysiological condition with excessive deposition of extracellular matrix and a relative lack of parenchymal cells (hepatocytes). Even if BMC transplantation is successful in supplying parenchymal cells, the fate of the extracellular matrix under these conditions is unknown. The present study clearly shows that transplanted BMCs reduce (degrade) carbon tetrachloride (CCl_4)-induced liver fibrosis with a significantly improved survival rate.

Materials and Methods

Mice. GFP-transgenic mice (TgN(β-act-EGFP)Osb) were kindly provided by Masaru Okabe (Genome Research Center, Osaka University, Osaka, Japan).[10] C57BL6 female mice were purchased from Japan SLC

Abbreviations: BMC, bone marrow cell; CCl4, carbon tetrachloride; GFP, green fluorescent protein; PBS, phosphate-buffered saline; IgG, immunoglobulin G; MMP, matrix metalloproteinase; NGS, normal goat serum; NRS, normal rabbit serum; DIG, digoxigenin.

From the [1]Department of Gastroenterology and Hepatology, School of Medicine, Yamaguchi University, Yamaguchi, Japan; and [2]Department of Physiological Chemistry, Graduate School of Pharmaceutical Science, University of Tokyo, Tokyo, Japan.

Received September 30, 2003; accepted August 16, 2004.

Supported in part by grants-in-aid 16590597, 12670490, and 10470136 from the Ministry of Education, Culture, Sports, Science and Technology and by grants-in-aid for translational research from the Ministry of Health, Labor and Welfare of Japan.

Address reprint requests to: Isao Sakaida, M.D., Department of Gastroenterology and Hepatology, School of Medicine, Yamaguchi University, Minami-Kogushi 1-1-1 Ube, Yamaguchi-pref. 755-8505, Japan. E-mail: sakaida@yamaguchi-u.ac.jp; fax: (81) 836-22-2240.

Published online in Wiley InterScience (www.interscience.wiley.com).

DOI 10.1002/hep.20452